FRAnCIs calculation program with universal Raman calibration data for the determination of PVX properties of CO2–CH4–N2 and CH4–H2O–NaCl systems and their uncertainties

Van-Hoan Le, Marie-Camille Caumon, Alexandre Tarantola

FRAnCIs calculation program with universal Raman calibration data for the determination of PVX properties of CO_2-CH_4-N_2 and CH_4-H_2O-NaCl systems and their uncertainties

Van-Hoan Le,[*] [a], Marie-Camille Caumon [a] and Alexandre Tarantola [a]

[a] Université de Lorraine, CNRS, GeoRessources Laboratory, BP 70239, F-54506 Vandoeuvre-lès-Nancy, France

[*] Corresponding author: van-hoan.le@univ-lorraine.fr

Authorship statement

V-H.L., M-C.C. and A.T. designed research; V-H.L. performed research and analyzed data; V-H.L., M-C.C. and A.T. wrote and revised the paper.

Abstract

Many experimental calibration data linking the variation of Raman spectral parameters (i.e., peak position, peak area/intensity ratio…) with the *PVX* properties of pure gases or mixtures of CO_2-CH_4-N_2 or CH_4-H_2O-NaCl systems have been published in literature by different laboratories. However, there is a significant discrepancy between these calibrations, leading possibly to inaccurate results when applied in another laboratory. In this paper, the inter-laboratory applicability of the existing calibration data is examined. Universal calibration data based on 78 regression equations and applicable for any Raman apparatus within any laboratory are provided in the form of a calculation program. The FRAnCIs (acronym for **F**luids: **R**aman **An**alysis of the **C**omposition of **I**nclusion**s**) Python user-friendly interface facilitates the application of these calibrations as well as to estimate the uncertainty of the measurements.

Keywords: Densimeter, Barometer, Fluid Inclusions, Raman Spectroscopy, *PVX* properties, FRAnCIs

Introduction

CH_4, CO_2 and N_2 are the main gaseous species present in natural geological fluids. Microthermometry is a standard method based on the observation of phase transition temperatures which is widely used to investigate the *PVTX* properties of geological fluids trapped within natural fluid inclusions (FI). The obtained microthermometry data are

interpreted using a proper thermodynamic model or an empirical equation of state (EoS) (Angus et al., 1976, 1978; Bakker and Diamond, 2000; Span and Wagner, 1996; Thiéry et al., 1994). Several computer programs integrating various common thermodynamic models and EoS have been developed for an ease-of-use such as FORTRAN, SALTY, Clathrates, AqSo_NaCl programs and HokieFlincs Excel spreadsheet for calculating the *PVX* properties of H_2O-CO_2-CH_4-N_2-NaCl-KCl-$CaCl_2$ system (Nicholls and Crawford, 1985; Bodnar et al., 1989; Bakker, 1997, 2018, 2019, Steele-MacInnis et al., 2012).

Microthermometry has however some limitations, for instance this method is difficult to apply in the case of small size (<5µm) fluid inclusions, or in the case of a gas phase of low density where no phase transitions might be observed, or also where not enough phase transitions are detected to resolve complex chemical compositions. For all these cases, Raman spectroscopy represents a powerful alternative (Rosso and Bodnar, 1995; Yamamoto and Kagi al., 2006, Song et al., 2009). Experimental Raman calibration data demonstrated that the pressure-induced frequency shift of the CH_4 ν_1 stretching band, of the CO_2 Fermi diad splitting and their peak area ratio are the most reliable spectral parameters for monitoring pressure (P), density (ρ), and composition (X) of fluid inclusions (Wright and Wang, 1973; Fabre and Oksengorn, 1992; Seitz et al., 1993, 1996). Thereby, numerous densimeters and barometers in the form of polynomial regression equations were provided not only for pure CO_2 and CH_4 but also for CH_4-CO_2-N_2 binary and ternary mixtures over different pressure-composition ranges (Seitz et al., 1993, 1996; Lin et al., 2007; Lu et al., 2007; Wang et al., 2011; Fall et al., 2011; Sublett et al., 2020, 2021; Le et al., 2019, 2020). Besides, the variation of the peak area ratio of CH_4 and H_2O (A_{CH_4}/A_{H_2O}) was also calibrated within CH_4-H_2O-NaCl system as a function of pressure, salinity and temperature to quantify dissolved CH_4 in the aqueous phase (Roedder and Bodnar, 1980; Ramboz et al., 1982; Pichavant et al., 1982; Dubessy et al., 2001; Guillaume et al., 2003; Caumon et al., 2014). All published calibration data were tested on natural fluid inclusions and validated by comparing the Raman results to those derived from microthermometry experiments.

However, the measured spectral parameters (e.g., peak position) were demonstrated to be instrument dependent (Lu et al., 2007; Lamadrid et al., 2017; Le et al., 2020). The aforementioned calibration data were then only validated for the specific Raman apparatus used upon its establishment. Indeed, the noticeable discrepancy between the densimeters and barometers existing in literature can lead to a significant difference of the estimated pressure

or density, depending on which densimeter or barometer is used (Lu et al., 2007; Lamadrid et al., 2017; Remigi et al., 2021).

Lu et al. (2007) compared nine experimental data sets based on the variation of the CH_4 ν_1 band position (at ~2917 cm^{-1}), then concluded that the unified calibration data should be established from the *relative* variation of the CH_4 ν_1 band position ($\nu^*_{CH_4}$), with $\nu^*_{CH_4} = \nu_{CH_4} - \nu^0_{CH_4}$ (where ν_{CH_4} and $\nu^0_{CH_4}$ are the fitted peak position of CH_4 ν_1 band measured at a given pressure and near-zero pressure, respectively). Besides, there is always a noticeable discrepancy between the measured spectral values of analyses repeated over different periods of time, even with identical instruments and settings within the same laboratory. This is likely due to a spontaneous drift in the response of the Raman apparatus upon different analytical sessions (Lamadrid et al., 2017; Sublett et al., 2020; Le et al., 2019, 2020). The use of $\nu^*_{CH_4}$ (instead of the absolute peak position of CH_4 ν_1 band, ν_{CH_4}) can therefore eliminate the spontaneous drift and so significantly improve the reproducibility of densimeters or barometers (Le et al., 2020).

Regarding the calibration data based on based on the variation of the CO_2 Fermi diad splitting (Δ), the reproducibility within the same laboratory (using identical Raman apparatus) is much better than that of the ν_{CH_4} measurement, even without any peak position correction (Fall et al., 2011; Le et al., 2020). However, the discrepancies between the resulting densimeters and barometers established within different laboratories are still significant, which should not be negligible upon accurate quantitative measurement of *PVX* properties (Lamadrid et al., 2017; Remigi et al., 2021). For assuring the highest accuracy of measurements, Lamadrid et al. (2017) recommended that researchers should develop their own calibration data which is specific and applicable only to their instruments and their data collection protocol.

Remigi et al. (2021) recently studied the inter-laboratory applicability using the bootstrapped confidence intervals (CIs). The authors showed that the spectral resolution is a prevailing parameter affecting the applicability of published CO_2 densimeters within different laboratories. By statistical comparison based on the measured CIs, the authors defined a set of rules that guide operators to choose an adequate calibration equation to their instrument configurations, and so extend the applicability of the published densimeter equations to other laboratories. According to their, the CO_2 densimeters can be applied in other laboratories (i) when a similar spectral resolution is used and for a limited density range, i.e., at above ~ 0.46

or 0.37 g·cm^{-3} depending on the used spectral resolution. The latter restriction significantly reduces the applicability of the published densimeters.

In this paper, the inter-laboratory applicability of the calibration data is evaluated by comparing the investigations published over the past ~30 years by different research groups using different Raman apparatus and configurations. New universal regression calibration equations that ensure the applicability of the calibration equation to any laboratories or Raman instruments are then provided for pure, binary and ternary systems of CO_2-CH_4-N_2. Since a large number of the regression calibration equations have been specifically provided for different pressure-composition ranges, and at different measurement temperatures, it is not convenient and practical to manually select the adequate calibration equation for a specific analysis. Also, the calculation of the *PVX* properties of gas mixtures from the Raman spectroscopic data involves an uncertainty estimation step. The latter is quite complex and time-consuming because the error propagation must consider several error sources, i.e., (i) the uncertainty of the measurement and determination of each spectral parameter (peak area, peak position) and (ii) the uncertainty arising from the regression polynomial equations themselves. We have thus developed a calculation program with a user-friendly interface (named FRAnCIs, acronym for **F**luids: **R**aman **An**alysis of the **C**omposition of **I**nclusion**s**) to facilitate the use of these universal calibration data upon daily analyses procedure. The most recent and complete calibration data for the determination of the dissolved CH_4 concentration within CH_4-H_2O-NaCl system is also assembled. Thereby, all quantitative calibration data including 78 regression polynomial equations are integrated within the FRAnCIs program for the determination of *PVX* properties and its uncertainty, directly from Raman spectroscopic data.

1. Universal calibration data

1.1. Applicability of the calibration data based on the variation of the CH_4 peak position

The applicability to various Raman apparatus and laboratories of the calibration data based on the variation of the peak position of the CH_4 ν_1 band (ν_{CH_4}) as a function of pressure and composition is evaluated herein by comparing a set of ten densimeters of pure CH_4 developed by different research groups over a long period of time. The instrumental configurations (i.e., laser, slit, hole, grating and objectives) and the temperature used upon the experimental measurements are all listed in Table 1.

125 Table 1 : Instrumental configurations used upon the establishment of the calibration data of ν_{CH_4}.

Reference	λ / nm	*T* / °C	Grating grooves/mm	Slit/hole / μm	Res. / cm^{-1}	Obj. Mag./N.A.
Fabre et al. (1992)*	488	22	nr	nr/nr	0.8	Nr
Seitz et al. (1993)*	514	23	1800	500/nr	4.4	50×/0.55
Thieu et al. (2000)	514	25	2400	nr/nr	nr	20×/nr
Lin et al. (2007)	514	22	1800	150/400	1.37	3.5×/0.1
Lu et al. (2007)	532	22	1800	nr/nr	1	40×/0.25
Zhang et al. (2016)	532	25	1800	50/-	0.65	50×/0.50
Fang et al. (2018)	532	22	1800	nr/nr	0.2	50×/0.35
Sublett et al. (2021)**	514	22	1800	150/400	nr	40×/0.55
Le et al. (2020)**	514	22, 32	1800	200/1000	1.7	20×/0.40

126 Calibration data were also provided for (*) CH_4-N_2 or CH_4-CO_2 binary and/or (**) CO_2-CH_4-N_2 ternary
127 mixture(s).
128 Res. - Spectral resolution, Obj. - Objective, Mag. - Magnification, N.A. - Numerical aperture, nr - not
129 reported.

130 1.1.1. Evaluation of the inter-laboratory applicability of existing calibration data

131 Most densimeters and barometers available in literature were developed by establishing
132 the relationship between ν_{CH_4} and density (or pressure) (Figure 1). In general, the overall
133 shape of these calibration curves is in good agreement. However, a noticeable separation is
134 observed, implying the modest reproducibility over different laboratories in the determination
135 of the *absolute* value of the peak position (ν_{CH_4}) (Lu et al., 2007). Namely, at near zero-
136 pressure, the maximum difference of the intercepts of these curves is about 2 cm^{-1} (Figure 1)
137 which can cause a fluctuation of up to ~ 0.1 $g \cdot cm^{-3}$ to the measured density.

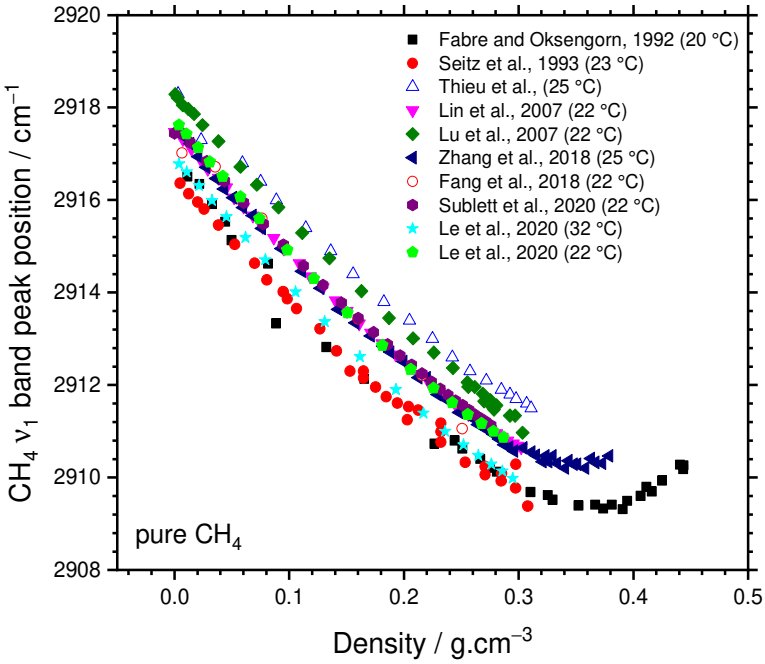

Figure 1 : Comparison of densimeters of pure CH_4 developed by different laboratories. The densimeter is based on the variation of the CH_4 band position (ν_{CH_4}) as a function of density.

A similar discrepancy is also observed when the calibration curves are established over different periods of time in the same laboratory with exactly the same instruments and configurations (Lamadrid et al., 2017; Le et al., 2020; Sublett et al., 2020). For instance, the calibration curves based on the variation of ν_{CH_4} within CH_4-N_2 mixtures of 70, 80 or 90 mol% CH_4 repeated over a period of ~ 1 - 4 months are not superimposed but are parallel with a separation of up to ~ 0.3 cm^{-1} (cf. Figure 3a in Le et al. 2020). Moreover, the calibration curves of the mixtures of 80 and 90 mol% CH_4 are indistinguishable (cf. Figure 3a in Le et al. 2020), indicating a significant error of up to ~ 0.6 cm^{-1}. The latter fluctuation may be attributed to the spontaneous drifts in the response of the spectrometer within different analytical sessions. Although the fluctuation between the calibration curves performed repeatedly in *the same laboratory* (up to ~ 0.6 cm^{-1}) are much smaller than the separation between the calibration curves performed by *different laboratories* (up to 2 cm^{-1}), the resulting errors arising from these fluctuations are still important, i.e., up to 150 bar for the pressure determination over the range 5 - 600 bar (corresponding a relative error of > 25%) and are expected to be even higher over a wider pressure (or density) range.

156 1.1.2. Unifying experimental calibration data by the relative variation of CH_4 band position

157 Although the discrepancy between the densimeters based on the variation of ν_{CH_4} has
158 been reported in Lu et al. (2007), this spectral parameter was still recently being used to
159 provide new densimeters or barometers, e.g., for pure CH_4 (Sublett et al., 2020) or for CH_4-
160 H_2 mixtures (Fang et al., 2018), etc., whereas its inter-laboratory applicability is not entirely
161 assured. Sublett et al. (2020, 2021) suggested a way to maintaining the consistency of
162 measurements, i.e., measuring the CH_4 ν_1 band position at 120 bar and 22 °C, then compare
163 to a "standard value" of their pure gas calibration curve for CH_4. The difference between
164 these two values is then used for peak position correction. However, it is noteworthy that the
165 spontaneous drift and the pressure-induced frequency shift of the CH_4 ν_1 band within pure
166 and mixtures of different concentrations may be not identical. As an evidence, their peak
167 positions of the CH_4 and N_2 bands at near zero-pressure (after being corrected by this mean)
168 still shows noticeable fluctuation of up to ~ 0.3 cm^{-1} (cf. Figure 2a and 4a in Sublett et al.
169 2021). Indeed, at near-zero pressure (density), the intermolecular distance is large enough as
170 such the gaseous molecules are considered to be nearly independent with no interaction with
171 surrounding molecules. Therefore, the effect of composition is negligible and so the peak
172 position of the CH_4 (and N_2) ν_1 band must theoretically have the same value. Any fluctuation
173 of the fitted (and corrected) peak position value of CH_4 and N_2 band at near zero-pressure can
174 thus be considered as analytical measurement errors. Thus, the peak position correction
175 should be done using the $\nu^0_{CH_4}$ (cf. Equation 1) rather than a "standard value" at high
176 pressure, e.g., 120 bar as suggested in Sublett et al. 2020. The reproducibility in the
177 measurements of the *relative* variation of the CH_4 ν_1 band position ($\nu^*_{CH_4}$, cf. Equation 1) is
178 much better than that of the absolute one, ν_{CH_4}, as experimentally demonstrated in Lu et al.
179 (2007) et Le et al. (2020).

$$\nu^*_{CH_4} = \nu_{CH_4} - \nu^0_{CH_4} \qquad 1$$

180 We recalculated the values of $\nu^0_{CH_4}$ for each published data set by extrapolating to near-
181 zero pressure (~ 1 - 5 bar), then listed in Table 2. All experimental data points based on ν_{CH_4}
182 were thereby converted to the *relative* variation of the CH_4 peak position ($\nu^*_{CH_4}$) and plotted
183 in Figure 2. Since the calibration curves are generally performed within one working day, the
184 systematic error and/or the day-to-day drift of the spectrometer (observed in Figure 1) could
185 therefore be reasonably eliminated. All calibration curves of pure CH_4 are now in good

agreement, except the data of Fang et al. (2018) (for unidentified reasons) and some data points of Seitz et al. (1993) (their experimental data are very scattered, perhaps due to the use of high spectral resolution, cf. Table 1). The separation between the calibration curves developed by different laboratories is now almost eliminated (Figure 2). For a given $\nu^*_{CH_4}$ value, the fluctuation of the density derived from these calibration curves for pure CH_4 is less than ~ 0.015 g·cm^{-3} for a density range between ~ 0.0 to 0.2 g·cm^{-3}, and less than ~ 0.02 g·cm^{-3} for density range from ~ 0.2 to 0.3 g·cm^{-3} (estimated by visual inspection).

Table 2 : Values of the peak position of the CH_4 ν_1 band measured at near-zero density ($\nu^0_{CH_4}$) derived from the published experimental calibration curves and used to determine the relative variation of the CH_4 band ($\nu^*_{CH_4}$).

References	T / °C	$\nu^0_{CH_4}$ / cm^{-1}
Fabre and Oskengorn (1992)	22	2916.50
Seitz et al. (1993)	23	2916.37
Thieu et al. (2000)	25	2918.60
Lin et al. (2007)	22	2917.47
Lu et al. (2007)	22	2918.20
Zhang et al. (2016)	25	2917.50
Fang et al. (2018)	22	2917.02
Sublett et al. (2020)	22	2917.45
Le et al. (2020)	22 and 32	2916.78 and 2917.63

Regarding the calibration curves developed within the same laboratory (i.e., using the same Raman apparatus and same instrumental settings), the fluctuation of the repeated calibration curves (based on $\nu^*_{CH_4}$) becomes significantly reduced, i.e., less than ~ 0.13 cm^{-1} (cf. Figure 3c in Le et al. 2020). The fluctuation of the densities derived from these repeated calibration curves is smaller than that observed in Figure 2, e.g., less than 0.01 g·cm^{-3} upon the density range from ~ 0 to 0.3 g·cm^{-3} (cf. Figure 4a in Le et al. 2020). The calibration data based on the *relative* variation of the CH_4 peak position ($\nu^*_{CH_4}$) then improves the reproducibility and can therefore be applied to any laboratory and/or to any Raman apparatus.

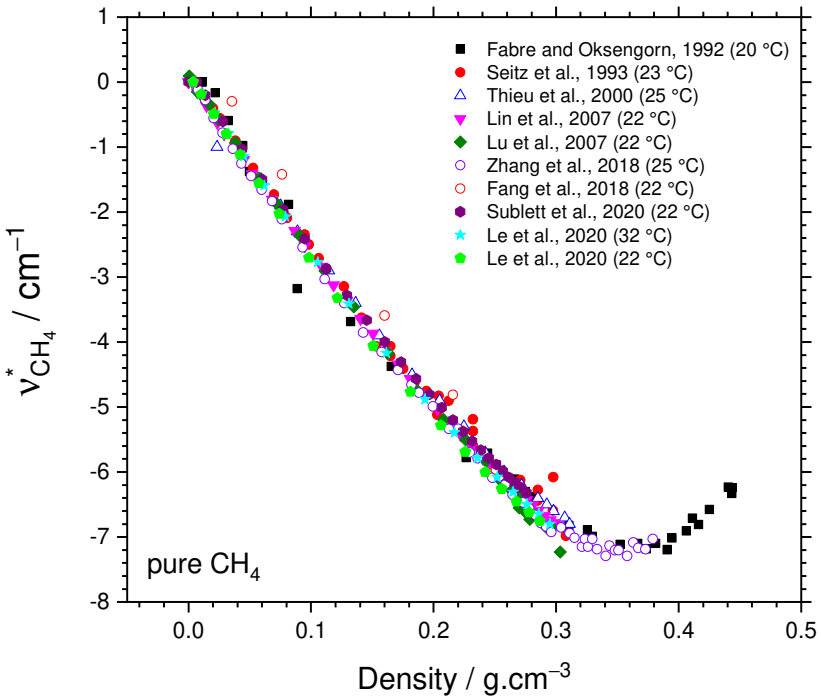

Figure 2 : Relative variation of the peak position of the CH_4 ν_1 band ($\nu^*_{CH_4}$) for pure CH_4 experiments.

A significant fluctuation (~ 0.85 cm^{-1}) of $\nu^0_{CH_4}$ is nevertheless observed even when the measurements are performed over different experimental sessions, even using the same instruments and configurations (Table 2; Le et al. 2020). Therefore, it is important to keep in mind that the accuracy of the determination of pressure or density using $\nu^*_{CH_4}$ can only be assured if the $\nu^0_{CH_4}$ value is accurately and properly determined. A sealed silica microcapillary containing less than ~ 5 bar of pure CH_4 is recommended as a standard for daily measurements of $\nu^0_{CH_4}$ (Le et al., 2020). The exact value of $\nu^0_{CH_4}$ must be measured at least at the beginning and at the end of the analytical session (we recommend every 3-5 analyses) for quantitative measurements of high quality that take into account any possible drift of the spectrometer.

Temperature also has an important effect on the relationship between $\nu^*_{CH_4}$ and pressure (Lin et al., 2007; Lu et al., 2007; Le et al., 2020). However, this effect on the variation of $\nu^*_{CH_4}$ as a function of density is subtle and can be negligible over the temperature range considered herein (from ~ 22 to 32 °C) (Figure 2). At higher temperature, the exact effect of temperature is still unclear. For instance, the experimental data of Zhang et al. (2016)

recorded over temperature range 25-200 °C shows a significant effect of temperature, whereas that of Lu et al. (2007) recorded over 22-200 °C do not show any effect. Thus, more attention should be paid to the measurement temperature.

1.1.3. Validity range of the calibration data based on $\nu^*_{CH_4}$

The experimental calibration data of pure CH_4 was reported for a pressure range up to ~ 3000 bar, corresponding to a density of ~ 0.45 g·cm^{-3} (Fabre and Oksengorn, 1992). An inflection point is observed at ~ 0.35 g·cm^{-3} on the calibration curve of pure CH_4 (Figure 2), implying that two values of density are possible for any given $\nu^*_{CH_4}$ when $\nu^*_{CH_4}$ is between ~ −6.2 and −7.3 cm^{-1}. Thus, another spectral parameter is required to constrain the actual density derived from the calibration curve. The FWHM (full width at half maximum) of the CH_4 ν_1 band is, among the other spectral parameters, the only one which continuously increases with increasing density or pressure, from near-zero density to 0.45 g·cm^{-3} (Figure 3). This parameter could therefore be potentially used to point out the correct density value between the two possibilities (before and after the inflection point of the calibration curves).

The variation of the FWHM of the ν_1 band of pure CH_4 experiments from five different research groups (as listed in Table 1) is plotted as a function of density in Figure 3a. The discrepancy between these experimental data sets is very similar to that observed for the densimeters (Figure 1a). Since the separation between the data sets may be large (up to 2.5 cm^{-1}), this parameter is not reliable and cannot be used to constrain the actual density derived from regression equation. The *relative* variation of the FWHM of these five data sets was then examined by normalizing the *absolute* values of the FWHM measured at a given density to the value of the FWHM measured at near-zero density. Nevertheless, the obtained results are still in disagreement with a poor reproducibility (Figure 3b). Moreover, two data sets of Le et al. (2020) recorded at 22 and 32 °C using the same spectrometer and configurations also point out the slight temperature dependence of the FWHM parameter (Figure 3b). This indicates that FWHM is highly sensitive not only to the variation of density (pressure) and temperature, but also depends on the measurement configurations and to the response of each instrument (Table 1). Consequently, the FWHM should neither be used as a reliable quantitative parameter, nor as an additional factor to point out the actual density derived from a given $\nu^*_{CH_4}$ between ~ −6.2 and −7.3 cm^{-1}. Besides, the value of $\nu^*_{CH_4}$ is nearly unchanged as the density varies from ~ 0.35 to 0.40 g·cm^{-3} (Figure 2a), implying that a small variation in

253 the measured $\nu^*_{CH_4}$ can result in a significant error of the measured density (pressure). In this
254 study, the validity range of the experimental calibration data is therefore restricted over the
255 density range 0 to ~ 0.35 g·cm^{-3}, i.e., just before the inflection point to ensure the reliability
256 of the calibration curve.

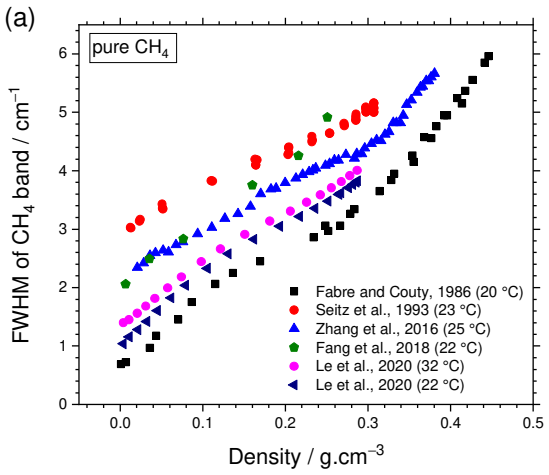

257

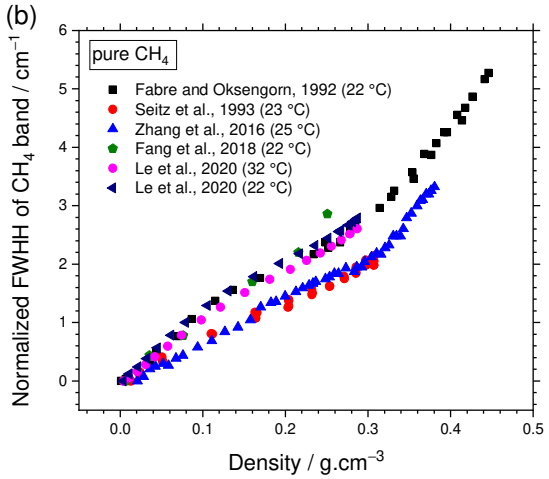

258

259 Figure 3 : (a) Variation of the measured FWHM (full width at half maximum) or (b) the relative
260 normalized FWHM of the ν_1 band of pure CH_4 as a function of density.

261 Figure 4 presents the regression polynomial equation of the density-$\nu^*_{CH_4}$ relationship,
262 which is fitted from all experimental data points measured over the density range from 0 to ~
263 0.35 g·cm^{-3} (247 data points), corresponding to a maximal pressure of 1065 bar at 22 °C. The
264 mathematical formula of the regression equation is expressed by Equation 2. The uncertainty
265 of the density derived from this regression equation is always less than 0.016 g·cm^{-3} (derived
266 from the 95% confidence intervals).

$$\rho = -0.0373.\nu^*_{CH_4} + 0.0011\left(\nu^*_{CH_4}\right)^2 + 4.02328.10^4\left(\nu^*_{CH_4}\right)^3 + 5.84981.10^{-5}\left(\nu^*_{CH_4}\right)^4 \quad (2)$$

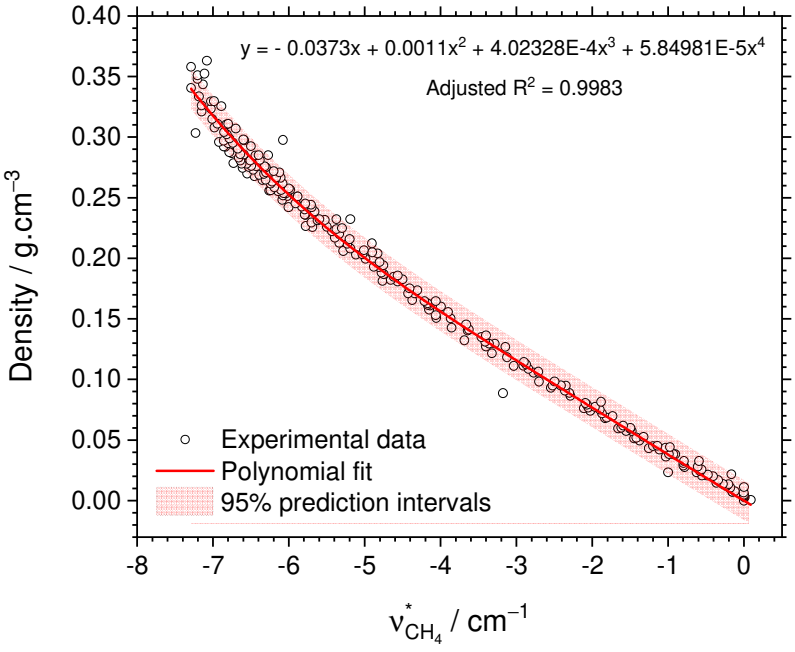

Figure 4 : Regression polynomial fit of the variation of $\nu^*_{CH_4}$ as a function of the density. This regression equation was fitted from the experimental data points reported by nine different research teams (Table 1) and can thus be used in other laboratory with confidence.

The published calibration data of CH_4-N_2 and CH_4-CO_2 **binary mixtures** covers a pressure range from ~ 5 to 600 bar, corresponding to a density of less than ~ 1.0 g·cm^{-3} depending on the mixture concentration (Seitz et al., 1996, 1993; Le et al., 2020). In this study, the experimental data of Seitz et al. (1993, 1996) are discarded because of the large dispersion of their data and the impossibility to accurately determine $\nu^0_{CH_4}$. Thus, only the calibration data of Le et al. (2020) provided over a pressure range of 5 - 600 bar are considered herein. The uncertainty of the pressure and density derived from theses calibration data is less than ± 20 bar and ± 0.02 g·cm^{-3}, respectively (Le et al., 2020). The mathematical formula of every regression calibration equations and associated coefficients fitted for each specific pressure-composition range and temperature will be all integrated in the FRAnCIs calculation program (see below).

1.2. Applicability of the calibration data based on the CO_2 Fermi diad splitting

1.2.1. Evaluation of the inter-laboratory applicability of the existing calibration data

Numerous densimeters or barometers based on the variation of the CO_2 Fermi diad splitting (Δ_{CO_2}) were published in literature for the direct estimation of the density or pressure of pure CO_2 (Wright and Wang, 1973; Garrabos et al., 1989; Rosso and Bodnar, 1995; Yamamoto and Kagi, 2006; Song et al., 2009; Wang et al., 2011; Fall et al., 2011; Lamadrid et al., 2018; Wang et al., 2019) and of CO_2-CH_4-N_2 binary or ternary mixtures (Seitz et al., 1996; Le et al., 2019, 2020). However, there is also a discernible discrepancy between these calibration data sets (Lamadrid et al., 2017; Wang et al., 2019), which is very similar to that observed between the densimeters of pure CH_4. In general, the calibration curves present a similar variation trend but are separated by a distance of up to ~ 0.1 cm^{-1} (Lamadrid et al., 2017; Remigi et al., 2021). Consequently, the density estimated from a given Δ_{CO_2} presents a substantial variation of up to 0.2 $g{\cdot}cm^{-3}$, depending on which densimeter is used.

Lamadrid et al. (2017) have carefully reassessed the difference between several densimeters of pure CO_2 available in the literature. Various potential causes such as (i) the variety of instrumentation, (ii) the difference in the data collection and processing, and (iii) the temporal variations were examined. The reproducibility in the measurement of Δ_{CO_2} performed over a long period (~ 4 years), as well as the applicability of the published densimeters of pure CO_2 were thereby assessed. The authors addressed some crucial remarks and conclusions. First, *Ne emission lines must be simultaneously recorded and used for wavenumber corrections to minimize the error in the determination of the fitted peak position of the two main bands of CO_2 (at 1388 and 1285 cm^{-1}, respectively).* According to the experimental data of our previous works (Le et al., 2019, 2020) which were performed during more than two years using the same Raman apparatus and configurations, it was noticed that the wavelength correction (using Ne emission lines) is not necessary because the parameter of interest herein is Δ_{CO_2}, not the position of individual bands of CO_2. The only requirement is that these two bands must be recorded simultaneously within a single measurement. As these CO_2 bands were simultaneously recorded over a small spectral window, all external errors affected to these two fitted band positions can potentially be identical, thus can be subtracted upon the measurement of Δ_{CO_2}. That is why the variation observed in our previous

study is quite small (~ 0.02 cm^{-1}), which is comparable with that observed in Lamadrid et al. (2017).

Second, Lamadrid et al. (2017) recommended that researchers should not use any calibration data in the literature due to the instrumental dependence of the calibration data, and that each laboratory should develop their own calibration data with their specific Raman apparatus. Notwithstanding, as demonstrated in previous section 1.1, the use of the relative band position variation ($\nu^*_{CH_4}$) could significantly increase the reproducibility and the inter-laboratory applicability of the obtained densimeters or barometers of pure CH_4 and CO_2-CH_4 and CH_4-N_2 mixtures. Thus, we believe that this normalization procedure can also be performed for the whole calibration data of CO_2 available in literature.

1.2.2. Unifying experimental calibration data based on the relative variation of CO_2 Fermi diad splitting

To examine the reproducibility and the applicability of the new densimeters and barometers based on the *relative* variation of the CO_2 Fermi diad splitting $\Delta^*_{CO_2}$ established by different laboratories, seven experimental calibration data sets of pure CO_2 were selected for comparison. The values of $\Delta^0_{CO_2}$ at near-zero density was determined from the intercept of each calibration curves at ~ 1-5 bar, and then listed in Table 3. The $\Delta^0_{CO_2}$ measured in our laboratory over two years present a variation of only ~ 0.02 cm^{-1} whereas that measured within various laboratories shows a fluctuation of up to ~ 0.1 cm^{-1} (Table 3). This indicates a significant impact of the instrumental factor on the reproducibility of the measurement of the CO_2 Fermi diad splitting, so on the inter-laboratory applicability of the experimental calibration data. For establishing the universal calibration data, $\Delta^*_{CO_2}$ at a given pressure (and temperature) is calculated from the *absolute* variation of the CO_2 Fermi diad splitting (Δ_{CO_2}) subtracted by the associated value of $\Delta^0_{CO_2}$ (Equation 3). The variation of the $\Delta^*_{CO_2}$ as a function of density or pressure was then plotted in Figure 5a and b, respectively.

$$\Delta^*_{CO_2} = \Delta_{CO_2} - \Delta^0_{CO_2} \qquad 3$$

Table 3 : CO_2 Fermi diad splitting at zero-pressure ($\Delta^0_{CO_2}$) determined from published experimental calibration curves.

References	*T* / °C	$\Delta^0_{CO_2}$ / cm^{-1}

Wang et al. (2011)	21	102.710
Fall et al. (2011)	35	102.651
Lamadrid et al. (2017)	23	102.630
Wang et al. (2019)	25	102.734
Wang et al. (2019)	40	102.719
Sublett et al. (2020)	22	102.667
Le et al. (2019, 2020)	22 and 32	102.75 ± 0.02

339

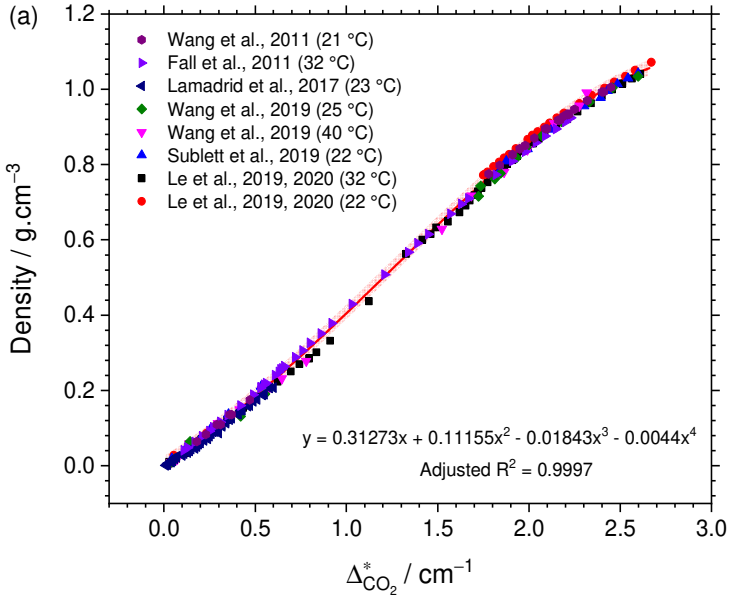

340

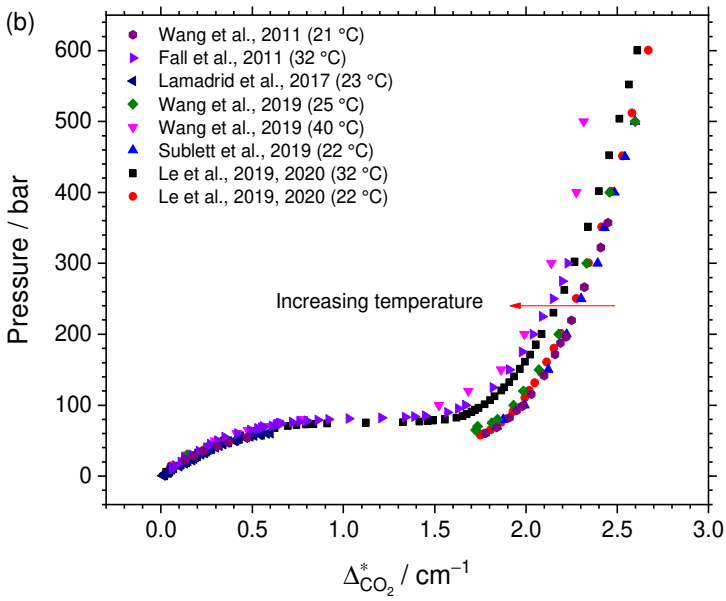

341

342 Figure 5 : Relative variation of the CO_2 Fermi diad splitting ($\Delta^*_{CO_2}$) within pure CO_2 as a function
343 of (a) density or (b) pressure and temperature. Overall, all densimeters based on the variation of $\Delta^*_{CO_2}$
344 are in good agreement, indicating the good inter-laboratory applicability. The temperature effect on
345 the variation of $\Delta^*_{CO_2}$ as a function of density is subtle and can be considered as negligible (21 °C -
346 40°C). The red-solid line in Figure (a) is the regression polynomial which was fitted from all
347 experimental data points (Equation 4).

348 These new universal densimeters are now nearly superimposed (Figure 5a). This implies
349 that the variation of the $\Delta^*_{CO_2}$ as a function of density do not depend on the laser nor on the
350 instrumental settings (such as the slit and/or the confocal aperture size, etc.). Namely, the
351 difference of the density derived from these new calibration curves is less than ~ 0.04 g·cm^{-3}
352 for the density region of 0.22 - 0.5 g·cm^{-3}, or less than 0.025 g·cm^{-3} for other regions.
353 Moreover, the effect of temperature on the $\Delta^*_{CO_2}$-density relationship is also subtle and can be
354 negligible, at least for temperatures range considered herein (i.e., between 21 and 40 °C).
355 Thus, a unique calibration equation was fitted from all these experimental data points (265
356 data points). The regression polynomial fit is presented by the red-solid line in Figure 5a and
357 expressed by Equation 4. The uncertainty of the predicted density is less than ~ ± 0.02 g·cm^{-3}
358 (estimated from the 95% confidence interval). The effect of temperature on the variation of
359 $\Delta^*_{CO_2}$ as a function of pressure is, however, more discernible and cannot be negligible (Figure
360 5b) which is similar to the $\nu^*_{CH_4}$-pressure relationship.

$$\rho = 0.31273\Delta^*_{CO_2} + 0.11155\left(\Delta^*_{CO_2}\right)^2 - 0.01843\left(\Delta^*_{CO_2}\right)^3 - 0.0044\left(\Delta^*_{CO_2}\right)^4 \qquad 4$$

Similarly, the experimental data of any CO_2-CH_4-N_2 binary or ternary mixtures based on the variation of Δ_{CO_2} over a pressure range of 5-600 bar (Le et al., 2019, 2020) were converted to $\Delta^*_{CO_2}$ using Equation 3. The universal calibration data of the $\Delta^*_{CO_2}$-pressure relationship and the $\Delta^*_{CO_2}$-density relationship (at 32 °C) are plotted in Figure 6 and 7, respectively. The universal experimental data measured at 22 °C are very similar, hence not shown here. A sealed microcapillary containing less than ~ 5 bar of pure CO_2 is needed to be used as a standard for accurately measuring $\Delta^0_{CO_2}$. Again, $\Delta^0_{CO_2}$ must be measured at least twice at the beginning and at the end of the experimental session to prevent and correct any drift of the response of the spectrometer.

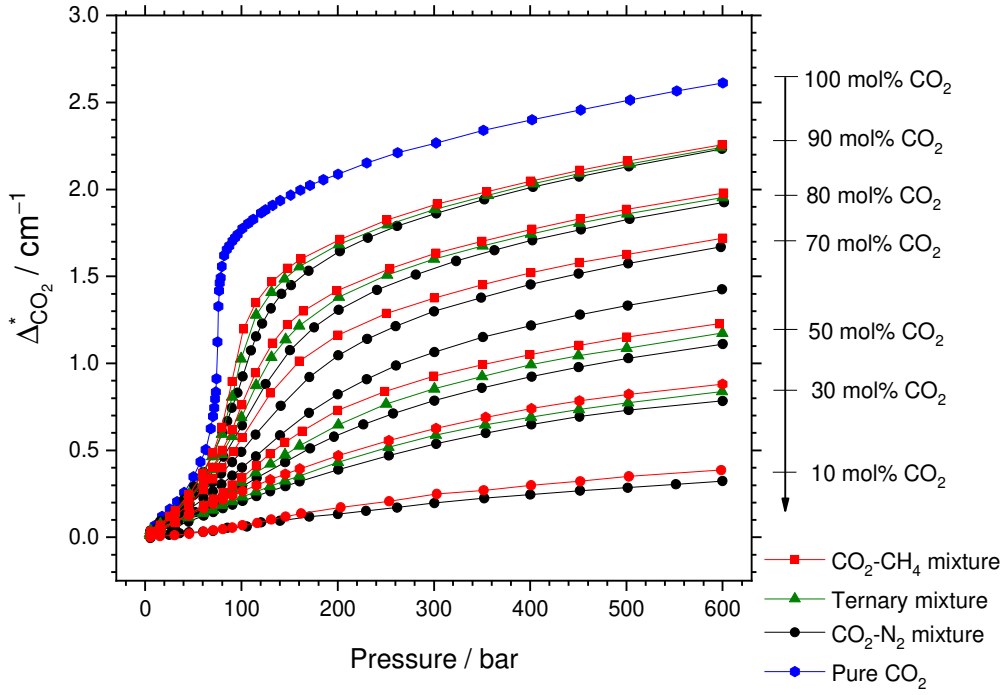

Figure 6 : Relative variation of the CO_2 Fermi diad splitting ($\Delta^*_{CO_2}$) as a function of pressure and composition within binary and ternary mixtures of CO_2-CH_4-N_2 measured in this study at 32 °C. The concentration of CO_2 within mixtures is directly indicated in the figure. The concentrations of CH_4 and N_2 within the ternary mixtures are equal. The calibration data obtained at 22 °C is similar and so not presented here.

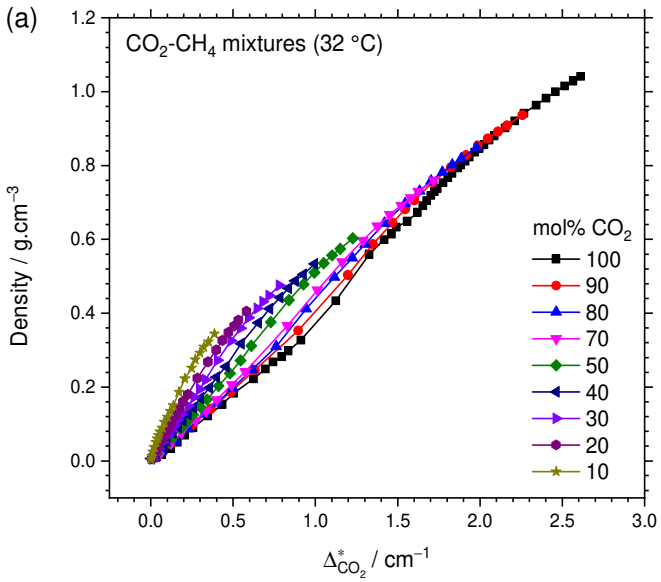

376

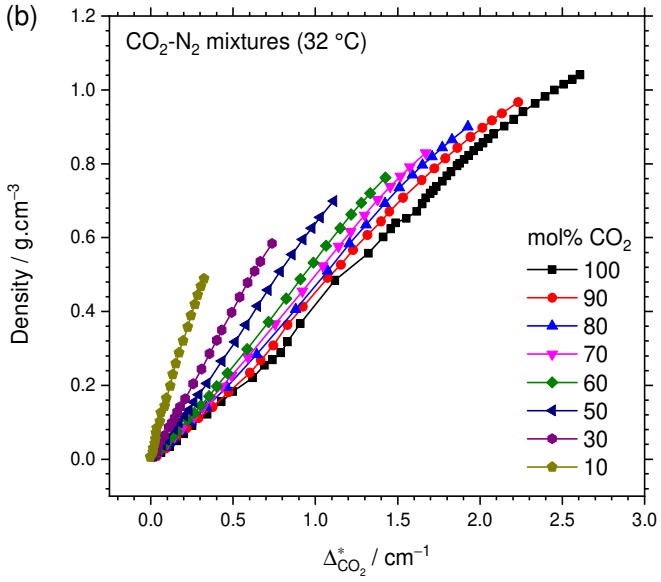

377

378 Figure 7 : Relative variation of the CO_2 Fermi diad splitting ($\Delta^*_{CO_2}$) as a function of density and
379 composition within (a) CO_2-CH_4 mixtures and (b) CO_2-N_2 mixtures (at 32 °C). The calibration data
380 obtained at 22 °C is similar and therefore not presented here.

381 Universal regression calibration equations were then fitted from these new calibration
382 data for the direct determination of the pressure and density of the CO_2-N_2 and CO_2-CH_4
383 binary and CO_2-CH_4-N_2 ternary gas mixtures. The mathematical formula of the regression
384 equation is expressed by Equation 5, where $\Delta^*_{CO_2}$ is the *relative* variation of the CO_2 Fermi
385 diad splitting. P and ρ are respectively the pressure (bar) and density (g·cm^{-3}) calculated from

a given composition X_{CO_2} (mol% CO_2) and $\Delta^*_{CO_2}$ (cm^{-1}). b_{ij} (with $i + j \leq 4$) are the fitting coefficients of the polynomial regression equations.

$$P\ (\text{or}\ \rho) = \sum_{i=0}^{3}\sum_{j=0}^{4} b_{ij} \cdot \left(X_{CO_2}\right)^i \cdot \left(\Delta^*_{CO_2}\right)^j \qquad 5$$

To minimize the uncertainty of the regression calibration equations, the experimental data were separately fitted for different concentration-pressure (or density) ranges. Thus, the coefficients b_{ij} in Equation 5 were correspondingly listed for each composition-pressure range within different tables in the Appendix A, i.e., Table A-1, A-2, A-3 and A-4 for the determination of pressure or density of the CO_2-CH_4 mixtures, and Table A-5, A-6, A-7 and A-8 for the determination of pressure or density of the CO_2-N_2 mixtures at 32 and 22 °C, respectively. The uncertainty (1σ) of the predicted pressure or density is also reported in the last row of each table.

2. FRAnCIs calculation program

2.1. Summary of all regression calibration equations and their validity range

Table 4 outlines the validity range of all regression polynomial calibration equations and associated uncertainty (1σ) and required spectral parameters of the regression calibration equations in the CO_2-CH_4-N_2 and CH_4-H_2O-NaCl systems which are considered herein.

Regarding the calibration data of CH_4, one set of regression polynomial calibration equations based on $\nu^*_{CH_4}$ was provided which can be used in different laboratories and with other Raman apparatus. The measurement of the $\nu^0_{CH_4}$ value (using a sample containing ~ 5 bar of CH_4) is mandatory in order to accurately calculate the $\nu^*_{CH_4}$. Regarding the calibration data of CO_2, two sets of calibration equations were provided. The first one is the original calibration data (based on Δ_{CO_2}) reported in Le et al. (2019, 2020). Hence, it is validated only for the Raman instruments of the authors' laboratory (GeoRessources, France) where the calibration data was established (measurements of $\Delta^0_{CO_2}$ is thus not required). The second set of calibration equations presented in section 2.2 and Appendix A is based on $\Delta^*_{CO_2}$, which are usable within other laboratories. The use of these calibration equations requires, however, the measurement of $\Delta^0_{CO_2}$.

Regarding the determination of the CH_4 dissolved content in CH_4-H_2O-NaCl system, we used the most recent and complete calibration data reported by Caumon et al. (2014) which is also in good agreement with previous studies (Lu et al., 2008; White, 2010). These calibration equations based on the peak area ratio A_{CH4}/A_{H2O} was fitted from more than 1000 data points, performed by different operators over one year, for a pressure range 30 - 1000 bar, temperature range 60 - 180 °C and the salinity range 0 - 4 mol.kg^{-1}. These regression equations are integrated into the FRAnCIs program for the determination of *PVX* properties and the estimation of the associated uncertainty directly from Raman spectroscopy data.

Table 4 : Recapitulation of the validity range (*TPρ* conditions), uncertainties, and required spectral parameters of the regression calibration equations in the CO_2-CH_4-N_2 and CH_4-H_2O-NaCl systems.

	T / °C	Spectral parameters required	*P* / bar	*ρ* / g·cm^{-3}	Nb of Eq.	Uncert. (1σ) / bar	Uncert. (1σ) / g·cm^{-3}
CO_2	21 - 40	Δ_{CO_2}, $\Delta^*_{CO_2}$	600	1.06	2	< 11	< 0.010
CH_4	22 - 35	$\nu^*_{CH_4}$	1140	0.35	2	-	< 0.010
CO_2-N_2	22, 32	Δ_{CO_2}, $\Delta^*_{CO_2}$	600	1.06*	32	< 10	< 0.006
CO_2-CH_4	22, 32	Δ_{CO_2}, $\Delta^*_{CO_2}$, $\nu^*_{CH_4}$	600	1.06*	24	< 12	< 0.008
CH_4-N_2	22, 32	$\nu^*_{CH_4}$	600	1.06*	16	< 18	< 0.006
CH_4-CO_2-N_2	22, 32	Δ_{CO_2}, $\Delta^*_{CO_2}$	600	1.06*	-	< 20	< 0.010
CH_4-H_2O-NaCl	60-180	A_{CH4}, A_{H2O}	1000	**	2	**	**

Nb of Eq. – the total number of calibration equations. Uncert. – uncertainty

* Up to ~ 1.06 g·cm^{-3}, depending on the composition of the gas mixtures.

** The CH_4 solubility is expressed in mol.kg^{-1} H_2O, the relative uncertainty of measured CH_4 solubility is between 5-10%.

2.2. General introduction of the calculation program – FRAnCIs

FRAnCIs (Fluids: Raman Analysis of the Composition of Inclusions) is a Python user-friendly calculation program developed to apply our calibration data. The program comprises seven independent calculation modules dedicatedly developed for a specific gas system (namely pure CO_2, pure CH_4, CO_2-N_2, CO_2-CH_4, CH_4-N_2 and CO_2-CH_4-N_2 mixtures, and CH_4-H_2O system) and listed in the "Start window" (Figure 8a). The relevant references of each module are listed at the bottom of the Start Window. The interface of each module is

slightly different (Figure 8b), depending on the required spectroscopic parameters, but in general contains four main sections: (i) recalling of all required spectral parameters, (ii) important remarks that must be taken into account upon performing the calculation, (ii) the INPUT field to enter the measured spectral parameters, and (iv) the OUTPUT field to display the final results and the associated uncertainties, i.e., composition (mol%), pressure (bar), density and molar volume (g·cm^{-3} and cm^3·mol^{-1}).

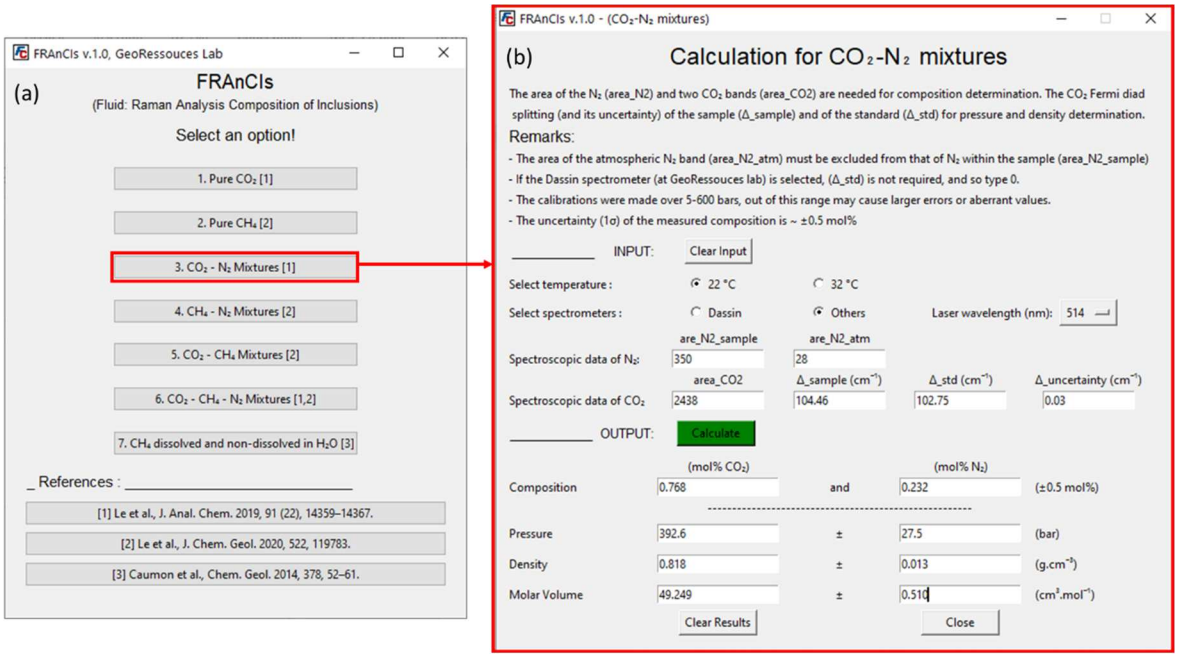

Figure 8 : User interface of the FRAnCIs program. (a) The starting window shows different options corresponding to different calculation modules developed specifically for each gas system, from pure to binary or ternary mixtures. The references for the corresponding calibration data are listed at the bottom of the first window. (b) Example of the interface of the calculation module for CO_2-N_2 mixtures.

2.3. Calculation procedure of *PVX* properties and estimation of global uncertainty

The calculation procedure and the estimation of uncertainty are somehow different depending on the selected gas system. Firstly, the concentration of the gas mixture is calculated from the fitted peak area and the corresponding relative Raman scattering cross-section (RRSCS) of each gaseous component. The value of the RRSCS of CO_2 and CH_4 was recently re-evaluated for the 514 nm excitation wavelength (Le et al., 2019, 2020). The RRSCS values for other excitation wavelengths are obtained using Equation 4.14 in Schrötter and Klöckner (1979) and all listed in Table 5. Once the concentration is calculated, the

pressure and the density of the gas mixture can be derived from the adequate calibration equations reported in previous sections.

Table 5 : RRSCS of CH_4 ν_1 band) and CO_2 (ν^+ and ν^- bands) for different wavelength excitations (nm) (Schrötter and Klöckner, 1979; Le et al., 2019, 2020)

	Peak position / cm^{-1}	σ 514 nm	σ^* 488 nm	σ^* 532 nm	σ^* 633 nm	σ^* 785 nm
CH_4 (ν_1)	2917	7.73 ± 0.16	7.80	7.69	7.44	7.05
CO_2 (ν^+)	1388	1.40 ± 0.04	1.41	1.39	1.35	1.28
CO_2 (ν^-)	1285	0.89 ± 0.03	0.89	0.88	0.85	0.81

All polynomial calibration equations are integrated into each calculation module of FRAnCIs program, thus can be automatically selected according to the composition-pressure ranges calculated from the input spectroscopic data. Since the RRSCS are laser-wavelength dependent, the user must select the corresponding laser used upon their experimental Raman analyses (cf. Figure 8b). The global uncertainty of the results is calculated by considering two main error sources:

The first error source, denoted as "i", arises from the uncertainty of the measured spectral parameters itself. This uncertainty component is mainly related to the efficiency of the instruments and how precise the researcher performs their Raman analyses. Indeed, the uncertainty on the determination of the spectral parameters can be estimated from repeated measurements at the same *PTX* conditions and the same instrumental configurations. According to the statistical analysis of the measurements performed with our Raman apparatus, the relative uncertainty of the measured peak area is about ± 0.4% of the absolute value of the fitted peak area leading to a global uncertainty of the measured composition is less than ~ ± 0.5 mol% (1σ) (cf. Appendix B for detailed uncertainty calculation). The later uncertainty is therefore used as the standard deviation of the composition measurement ($i_{X_{CO_2}}$) for any further calculation involving the concentration of the gas mixtures. On the other hand, the uncertainty of an individual fitted peak position measured in our study is about ~ ± 0.01 cm^{-1} (estimated from six repeated measurements), resulting in the uncertainty

of the measured CO_2 Fermi diad splitting ($i_{\Delta_{CO_2}}$) and the variation of the CH_4 peak position ($i_{\nu_{CH_4}}$) of about ~ ± 0.020 cm^{-1}.

The second error source, denoted as "u", is related to how well the best-fitted regression equation reproduces the pressure or the density from the measured composition and the CO_2 Fermi diad splitting (with uncertainty ± $i_{\Delta_{CO_2}}$) or the variation of the CH_4 peak position (with an uncertainty ± $i_{\nu_{CH_4}}$). The uncertainty component "u" was specifically derived from the 95% prediction intervals of each regression polynomial equation and listed in the last row of the tables given the fitted coefficients of each regression equation (Appendix A).

The global uncertainty of the final measured density or pressure considered herein is the sum of these two error sources (u + i). Since the regression calibration equations reported in this study are nonlinear, the uncertainty component i can cause either significant error or not, depending on the "slope" of the best-fitted curve or surface at the considered composition-density region. The detailed calculation procedure (including the uncertainty estimation) and examples of calculation for each system can be found in Appendix A.

3. Conclusion

Numerous experimental densimeters and barometers previously published in literature were collected and revised to examine their inter-laboratory applicability. The discrepancy of these densimeters and barometers was mainly attributed to the spontaneous and systematic day-to-day drift of the instrumental response. The *relative* variation of quantitative spectral parameters ($\nu^*_{CH_4}$ and $\Delta^*_{CO_2}$) is therefore used to establishing the universal regression calibration equations that are applicable in other laboratories and/or other Raman apparatus. Due to the day-to-day drift of the Raman spectrometer, the standard value of the CO_2 Fermi splitting and the CH_4 ν_1 band position at near-zero density ($\Delta^0_{CO_2}$ and $\nu^0_{CH_4}$) must be accurately determined at least twice, i.e., at the beginning and the end of the analysis session. More checks are also recommended during the analytical section (after every 3 to 5 measurement of samples) to prevent as soon as possible any minimal drift of the response of the spectrometers, and so to ensure the highest accuracy of the measurements.

FRAnCIs calculation program integrating all regression polynomial equations was developed to facilitate the application of our universal calibration data. Thereby, the final *PVX* properties of the sample and the associated global uncertainty can be conveniently

calculated from Raman spectroscopic data via a user-friendly interface. The program can be downloaded from the Supplementary Data section or by contacting the authors of the present paper. A sealed silica microcapillary containing less than ~ 5 bar of pure CH_4 or CO_2 are highly recommended to be used as standards for the routine calibration and for the accurate determination of the relative variation of peak position which is required by FRAnCIs program. In case you cannot make these capillary standards, GeoRessources lab can provide it (contact the authors for more detail). It is to note that, the admixture of additional gaseous species cannot be ignored because of the high sensitivity of the Raman spectral parameters to the chemical composition change. Therefore, the calibration data reported in this study can only be applied to the CO_2-CH_4-N_2 and/or CH_4-H_2O-NaCl systems. The calibration data for other specific gas mixtures must be dedicatedly developed to ensure a satisfactory uncertainty of the quantitative measurement of density and pressure.

Acknowledgements

This work is a part of the Ph.D thesis of Van-Hoan Le (Université de Lorraine) who acknowledges the French Ministry of Education and Research and the ICEEL Institute Carnot. The work benefited financial support from CNRS-INSU CESSUR program. The authors are grateful to Dr. Márta Berkesi and an anonymous reviewer for their constructive comments.

Computer code availability

Name: FRAnCIs

Developer: Van-Hoan Le, GeoRessources Laboratory, University of Lorraine, BP 70239, F-54506 Vandoeuvre-lès-Nancy, France, telephone number: +33 3 72 74 55 77

Email: van-hoan.le@univ-lorraine.fr

Year of first available: 2017

Software required: No

Program language: Python (v 3.8.1)

Program size: 18 Mb

License: https://opensource.org/licenses

Source code: https://github.com/vanhoanle92/FRAnCIs-calculation-program.git or can be found in Supplementary Data

References

Angus, S., Armstrong, B., de Reuck, K.M., 1978. International thermodynamic tables of the fluid state. 5. Methane.

Angus, S., Armstrong, B., De Reuck, K.M., Altunin, V.V., Gadetskii, O.G., Chapela, G.A., Rowlinson, J.S., 1976. International thermodynamic tables of the fluid state. Carbon Dioxide 3, 338–342.

Bakker, R.J., 2019. Package fluids. Part 5: The NaCl-H2O system in fluid inclusion research and applications of the software AqSo_NaCl (Bakker, 2018). Chem. Geol. 525, 400–413. https://doi.org/10.1016/j.chemgeo.2019.07.041

Bakker, R.J., 2018. AqSo_NaCl: Computer program to calculate p-T-V-x properties in the H 2 O-NaCl fluid system applied to fluid inclusion research and pore fluid calculation. Comput. Geosci. 115, 122–133. https://doi.org/10.1016/j.cageo.2018.03.003

Bakker, R.J., 1997. Clathrates: Computer programs to calculate fluid inclusion V-X properties using clathrate melting temperatures. Comput. Geosci. 23, 1–18. https://doi.org/10.1016/S0098-3004(96)00073-8

Bakker, R.J., Diamond, L.W., 2000. Determination of the composition and molar volume of H2O-CO2 fluid inclusions by microthermometry. Geochim. Cosmochim. Acta 64, 1753–1764. https://doi.org/10.1016/S0016-7037(99)00334-8

Bodnar, R.J., Sterner, S.M., Hall, D.L., 1989. SALTY: a FORTRAN program to calculate compositions of fluid inclusions in the system NaCl-KCl-H2O. Comput. Geosci. 15, 19–41. https://doi.org/10.1016/0098-3004(89)90053-8

Caumon, M.-C., Robert, P., Laverret, E., Tarantola, A., Randi, A., Pironon, J., Dubessy, J., Girard, J.-P., 2014. Determination of methane content in NaCl–H2O fluid inclusions by Raman spectroscopy. Calibration and application to the external part of the Central Alps (Switzerland). Chem. Geol. 378, 52–61. https://doi.org/10.1016/j.chemgeo.2014.03.016

Dubessy, J., Buschaert, S., Lamb, W., Pironon, J., Thiéry, R., 2001. Methane-bearing aqueous fluid inclusions: Raman analysis, thermodynamic modelling and application to petroleum basins. Chem. Geol., 7th Pan American Conference on Research on Fluid Inclusions 173, 193–205. https://doi.org/10.1016/S0009-2541(00)00275-8

Fabre, D., Oksengorn, B., 1992. Pressure and Density Dependence of the CH4 and N2 Raman Lines in an Equimolar CH4/N2 Gas Mixture. Appl. Spectrosc. 46, 468–471.

Fall, A., Tattitch, B., Bodnar, R.J., 2011. Combined microthermometric and Raman spectroscopic technique to determine the salinity of H2O–CO2–NaCl fluid inclusions based on clathrate melting. Geochim. Cosmochim. Acta 75, 951–964. https://doi.org/10.1016/j.gca.2010.11.021

Fang, J., Chou, I.-M., Chen, Y., 2018. Quantitative Raman spectroscopic study of the H2─CH4 gaseous system. J. Raman Spectrosc. 49, 710–720. https://doi.org/10.1002/jrs.5337

Garrabos, Y., Chandrasekharan, V., Echargui, M.A., Marsault-Herail, F., 1989. Density effect on the raman fermi resonance in the fluid phases of CO2. Chem. Phys. Lett. 160, 250–256. https://doi.org/10.1016/0009-2614(89)87591-8

579 Guillaume, D., Teinturier, S., Dubessy, J., Pironon, J., 2003. Calibration of methane analysis
580 by Raman spectroscopy in H2O–NaCl–CH4 fluid inclusions. Chem. Geol., European
581 Current Research on Fluid Inclusions 194, 41–49. https://doi.org/10.1016/S0009-
582 2541(02)00270-X

583 Lamadrid, H.M., Moore, L.R., Moncada, D., Rimstidt, J.D., Burruss, R.C., Bodnar, R.J.,
584 2017. Reassessment of the Raman CO2 densimeter. Chem. Geol. 450, 210–222.
585 https://doi.org/10.1016/j.chemgeo.2016.12.034

586 Lamadrid, H.M., Steele-Macinnis, M., Bodnar, R., 2018. Relationship between Raman
587 spectral features and fugacity in mixtures of gases. J. Raman Spectrosc.
588 https://doi.org/10.1002/jrs.5304

589 Le, V.-H., Caumon, M.-C., Tarantola, A., Randi, A., Robert, P., Mullis, J., 2020. Calibration
590 data for simultaneous determination of P-V-X properties of binary and ternary CO2 -
591 CH4 - N2 gas mixtures by Raman spectroscopy over 5–600 bar: Application to
592 natural fluid inclusions. Chem. Geol. 552, 119783.
593 https://doi.org/10.1016/j.chemgeo.2020.119783

594 Le, V.-H., Caumon, M.-C., Tarantola, A., Randi, A., Robert, P., Mullis, J., 2019. Quantitative
595 Measurements of Composition, Pressure, and Density of Microvolumes of CO2–N2
596 Gas Mixtures by Raman Spectroscopy. Anal. Chem. 91, 14359–14367.
597 https://doi.org/10.1021/acs.analchem.9b02803

598 Lin, F., Bodnar, R.J., Becker, S.P., 2007. Experimental determination of the Raman CH4
599 symmetric stretching (ν1) band position from 1–650bar and 0.3–22°C: Application to
600 fluid inclusion studies. Geochim. Cosmochim. Acta 71, 3746–3756.
601 https://doi.org/10.1016/j.gca.2007.05.016

602 Lu, W., Chou, I.M., Burruss, R.C., 2008. Determination of methane concentrations in water
603 in equilibrium with sI methane hydrate in the absence of a vapor phase by in situ
604 Raman spectroscopy. Geochim. Cosmochim. Acta 72, 412–422.
605 https://doi.org/10.1016/j.gca.2007.11.006

606 Lu, W., Chou, I.-M., Burruss, R.C., Song, Y., 2007. A unified equation for calculating
607 methane vapor pressures in the CH4–H2O system with measured Raman shifts.
608 Geochim. Cosmochim. Acta 71, 3969–3978.
609 https://doi.org/10.1016/j.gca.2007.06.004

610 Nicholls, J., Crawford, M.L., 1985. FORTRAN programs for calculation of fluid properties
611 from microthermometric data on fluid inclusions. Comput. Geosci. 11, 619–645.
612 https://doi.org/10.1016/0098-3004(85)90090-1

613 Pichavant, M., Ramboz, C., Weisbrod, A., 1982. Fluid immiscibility in natural processes: Use
614 and misuse of fluid inclusion data: I. Phase equilibria analysis — A theoretical and
615 geometrical approach. Chem. Geol., Current Research on Fluid Inclusions 37, 1–27.
616 https://doi.org/10.1016/0009-2541(82)90064-X

617 Ramboz, C., Pichavant, M., Weisbrod, A., 1982. Fluid immiscibility in natural processes: Use
618 and misuse of fluid inclusion data: II. Interpretation of fluid inclusion data in terms of
619 immiscibility. Chem. Geol., Current Research on Fluid Inclusions 37, 29–48.
620 https://doi.org/10.1016/0009-2541(82)90065-1

621 Remigi, S., Mancini, T., Ferrando, S., Frezzotti, M.L., 2021. Inter-Laboratory Application of
622 Raman CO_2 Densimeter Equations: Experimental Procedure and Statistical Analysis

623 Using Bootstrapped Confidence Intervals. Appl. Spectrosc. 0003702820987601.
624 https://doi.org/10.1177/0003702820987601

625 Roedder, E., Bodnar, R.J., 1980. Geologic Pressure Determinations from Fluid Inclusion
626 Studies. Annu. Rev. Earth Planet. Sci. 8, 263–301.
627 https://doi.org/10.1146/annurev.ea.08.050180.001403

628 Rosso, K.M., Bodnar, R.J., 1995. Microthermometric and Raman spectroscopic detection
629 limits of C02 in fluid inclusions and the Raman spectroscopic characterization of C02.
630 Geochim. Cosmochim. Acta 59, 3961–3975. https://doi.org/10.1016/0016-
631 7037(95)94441-H

632 Schrötter, H.W., Klöckner, 1979. Raman Scattering Cross Section in Gases and Liquids, in:
633 Topics in Current Physics. pp. 123–164.

634 Seitz, J.C., Pasteris, J.D., Chou, I.-M., 1996. Raman spectroscopic characterization of gas
635 mixtures. II. Quantitative composition and pressure determination of the CO2-CH4
636 system. Am. J. Sci. 296, 577–600.

637 Seitz, J.C., Pasteris, J.D., Chou, I.-M., 1993. Raman spectroscopic characterization of gas
638 mixtures; I, Quantitative composition and pressure determination of CH 4, N 2 and
639 their mixtures. Am. J. Sci. 293, 297–321.

640 Song, Y., Chou, I., Hu, W., Robert, B., Lu, W., 2009. CO2 Density-Raman Shift Relation
641 Derived from Synthetic Inclusions in Fused Silica Capillaries and Its Application.
642 Acta Geol. Sin. - Engl. Ed. 83, 932–938. https://doi.org/10.1111/j.1755-
643 6724.2009.00090.x

644 Sublett, D.M., Sendula, E., Lamadrid, H., Steele-MacInnis, M., Spiekermann, G., Burruss,
645 R.C., Bodnar, R.J., 2020. Shift in the Raman symmetric stretching band of N2, CO2,
646 and CH4 as a function of temperature, pressure, and density. J. Raman Spectrosc. 51,
647 555–568. https://doi.org/10.1002/jrs.5805

648 Sublett, D.M., Sendula, E., Lamadrid, H.M., Steele-MacInnis, M., Spiekermann, G., Bodnar,
649 R.J., 2021. Raman spectral behavior of N2, CO2, and CH4 in N2–CO2–CH4 gas
650 mixtures from 22°C to 200°C and 10 to 500 bars, with application to other gas
651 mixtures. J. Raman Spectrosc. 52, 750–769. https://doi.org/10.1002/jrs.6033

652 Span, R., Wagner, W., 1996. A New Equation of State for Carbon Dioxide Covering the
653 Fluid Region from the Triple-Point Temperature to 1100 K at Pressures up to 800
654 MPa. J. Phys. Chem. Ref. Data 25, 1509–1596. https://doi.org/10.1063/1.555991

655 Steele-MacInnis, M., Lecumberri-Sanchez, P., Bodnar, R.J., 2012. HokieFlincs_H2O-NaCl:
656 A Microsoft Excel spreadsheet for interpreting microthermometric data from fluid
657 inclusions based on the PVTX properties of H2O–NaCl. Comput. Geosci. 49, 334–
658 337. https://doi.org/10.1016/j.cageo.2012.01.022

659 Thieu, V., Subramanian, S., Colgate, S.O., Sloan, E.D., 2000. High-Pressure Optical Cell for
660 Hydrate Measurements Using Raman Spectroscopy. Ann. N. Y. Acad. Sci. 912, 983–
661 992. https://doi.org/10.1111/j.1749-6632.2000.tb06853.x

662 Thiéry, R., Kerkhof, A., Dubessy, J., 1994. vX properties of CH4 -CO2 and CO2 -N2 fluid
663 inclusions; modelling for T<31 degrees C and P<400 bars. Eur. J. Mineral. 6, 753–
664 771.

665 Wang, W., Caumon, M.-C., Tarantola, A., Pironon, J., Lu, W., Huang, Y., 2019. Raman
666 spectroscopic densimeter for pure CO2 and CO2-H2O-NaCl fluid systems over a

667 wide P-T range up to 360 °C and 50 MPa. Chem. Geol. 528, 119281.
668 https://doi.org/10.1016/j.chemgeo.2019.119281

669 Wang, X., Chou, I.-M., Hu, W., Burruss, R.C., Sun, Q., Song, Y., 2011. Raman spectroscopic
670 measurements of CO2 density: Experimental calibration with high-pressure optical
671 cell (HPOC) and fused silica capillary capsule (FSCC) with application to fluid
672 inclusion observations. Geochim. Cosmochim. Acta 75, 4080–4093.
673 https://doi.org/10.1016/j.gca.2011.04.028

674 White, S.N., 2010. Qualitative and Quantitative Analysis of CO2 and CH4 Dissolved in
675 Water and Seawater Using Laser Raman Spectroscopy. Appl. Spectrosc. 64, 819–827.
676 https://doi.org/10.1366/000370210791666354

677 Wright, R.B., Wang, C.H., 1973. Density effect on the Fermi resonance in gaseous CO2 by
678 Raman scattering. J. Chem. Phys. 58, 2893–2895. https://doi.org/10.1063/1.1679594

679 Yamamoto, J., Kagi, H., 2006. Extended Micro-Raman Densimeter for CO2 Applicable to
680 Mantle-originated Fluid Inclusions. Chem. Lett. 35, 610–611.
681 https://doi.org/10.1246/cl.2006.610

682 Zhang, J., Qiao, S., Lu, W., Hu, Q., Chen, S., Liu, Y., 2016. An equation for determining
683 methane densities in fluid inclusions with Raman shifts. J. Geochem. Explor., Fluid
684 and Melt inclusions 171, 20–28. https://doi.org/10.1016/j.gexplo.2015.12.003

Appendix A: Coefficients of regression calibration equations

Table A-1: Fitted coefficients of Equation 5 for the determination of pressure (at 32 °C) of CO_2-CH_4 gas mixtures. The uncertainty (1σ) of the calibration polynomial equation of each range is listed in the last row.

PX domains / c_{ij}	50-100 mol% CO_2		10-50 mol% CO_2	
	5-600 bar	5-160 bar	5-600 bar	5-160 bar
c00	–105.913	141.952	20.141	54.201
c10	631.841	–579.239	119.317	–579.442
c01	1192.786	614.574	1735.798	2003.442
c20	–1078.549	760.306	–1063.462	1889.818
c11	–4347.619	–598.096	–10364.644	–5145.786
c02	758.153	–207.733	1503.426	–4786.568
c30	554.031	–322.119	1503.573	–1886.673
c21	6980.102	255.994	33241.615	456.077
c12	–3305.090	–483.570	–14970.863	19020.925
c03	631.878	401.280	3045.567	1651.598
c31	–3652.934	–109.853	–35823.587	6424.637
c22	2458.432	637.310	22248.061	–18744.547
c13	679.754	–475.666	–5471.870	–5277.348
c04	34.686	40.255	80.945	1174.052
Adjusted R^2	0.9993	0.9988	0.9989	0.9951
Uncertainty (1σ)	± 5 bar	± 3 bar	± 10 bar	± 4 bar

692 Table A-2: Fitted coefficients of Equation 5 for the determination of density (at 32 °C) of CO_2-
693 CH_4 gas mixtures. The uncertainty (1σ) of the calibration polynomial equation of each range is listed
694 in the last row.

PX domains / c_{ij}	50-100 mol% CO_2		10-50 mol% CO_2	
	5-600 bar	5-160 bar	5-600 bar	5-160 bar
c00	0.267075	0.254772	0.062867	0.047241
c10	–1.169842	–1.082592	–0.683745	–0.543798
c01	0.816076	0.762897	1.281116	1.582450
c20	1.651565	1.481580	2.274286	1.857576
c11	–0.872643	–0.893355	–1.634755	–2.644046
c02	–0.055892	0.113777	–0.901265	–3.137805
c30	–0.745041	–0.658874	–2.317295	–1.907131
c21	0.1121156	0.673482	–4.154535	–5.118171
c12	0.7575122	–0.138406	5.889787	18.341107
c03	–0.1854704	0.027368	–0.595327	–1.806949
c31	0.2196812	–0.161483	8.311497	11.389876
c22	–0.5740299	–0.100446	–7.983288	–21.602594
c13	0.1726441	0.156471	1.397482	0.245593
c04	–0.0071123	–0.055429	–0.102337	1.535738
Adjusted R^2	0.9997	0.9996	0.9996	0.9980
Uncertainty (1σ)	± 0.006	± 0.005	± 0.003	± 0.004

695

Table A-3: Fitted coefficients of Equation 5 for the determination of pressure (at 22 °C) of CO_2-CH_4 gas mixtures. The uncertainty (1σ) of the calibration polynomial equation of each range is listed in the last row.

PX domains / c_{ij}	50-100 mol% CO_2		10-50 mol% CO_2	
	5-600 bar	5-160 bar	5-600 bar	5-160 bar
c00	178.110	63.138	45.382	–18.197
c10	–493.276	–229.832	–437.060	291.460
c01	174.125	409.524	–13.891	853.921
c20	320.292	268.950	1379.635	–1096.748
c11	–580.958	–52.822	9096.755	413.727
c02	773.463	–154.154	–385.162	–1397.053
c30	–1.111	–101.463	–1398.590	1181.763
c21	2655.985	–352.855	–33996.147	–7348.360
c12	–3584.041	–417.642	–2105.436	5112.146
c03	654.829	307.936	2163.473	249.588
c31	–2100.462	147.065	35077.079	9121.890
c22	2686.202	525.599	3647.292	–6356.070
c13	–669.269	–400.575	–3723.511	208.556
c04	26.174	45.434	95.283	–35.643
Adjusted R^2	0.9989	0.9987	0.9944	0.9987
Uncertainty (1σ)	±8 bar	±3 bar	±12 bar	±3 bar

Table A-4: Fitted coefficients of Equation 5 for the determination of density (at 22 °C) of CO_2-CH_4 gas mixtures. The uncertainty (1σ) of the calibration polynomial equation of each range is listed in the last row.

PX domains / c_{ij}	50-100 mol% CO_2		10-50 mol% CO_2	
	5-600 bar	5-160 bar	5-600 bar	5-160 bar
c00	–0.095144	0.042391	–0.028497	–0.015283
c10	0.388100	–0.163524	0.446167	0.250370
c01	0.627318	0.311039	0.823317	0.817400
c20	–0.479419	0.220851	–1.795601	–0.924644
c11	–0.314993	0.814068	–0.498819	–0.526408
c02	–0.019846	0.041350	0.067829	0.290467
c30	0.189601	–0.105147	2.075280	0.972751
c21	–0.723497	–1.843815	–0.668362	–3.491540
c12	0.873300	0.609623	0.985340	5.508150
c03	–0.216237	–0.199379	–0.587449	–3.529910
c31	0.683057	1.115065	–0.193511	6.275225
c22	–0.744117	–0.894715	–1.604829	–12.943609
c13	0.216532	0.467502	1.174957	8.131834
c04	–0.009033	–0.069460	–0.054438	–0.328421
Adjusted R^2	0.9998	0.9999	0.9994	0.9953
Uncertainty (1σ)	±0.006	±0.004	±0.006	±0.005

Table A-5: Fitted coefficients of Equation 5 for the determination of pressure (at 32°C) of CO_2-N_2 gas mixtures. The uncertainty (1σ) of the calibration polynomial equation of each range is listed in the last row.

PX domains / c_{ij}	50-100 mol% CO_2		10-50 mol% CO_2	
	5-600 bar	5-160 bar	5-600 bar	5-160 bar
c00	–141.222	44.653	–7.980	27.879
c10	682.710	–178.218	269.903	–309.341
c01	2377.959	1317.024	2587.526	2420.432
c20	–1033.802	228.764	–1224.785	1080.882
c11	–8587.547	–3376.477	–17336.257	–11059.840
c02	782.696	63.581	2115.167	–1531.374
c30	492.546	–94.070	1435.628	–1154.706
c21	11797.178	3759.578	49648.794	18759.022
c12	–2971.818	–848.445	–14261.990	11079.420
c03	533.510	348.836	2095.490	–2896.324
c31	–5410.457	–1534.820	–47522.157	–9353.915
c22	2092.099	721.810	18998.615	–17517.273
c13	–576.573	–415.550	–3716.869	7020.022
c04	33.948	38.401	110.044	–346.217
Adjusted R^2	0.9980	0.9983	0.9990	0.9924
Uncertainty (1σ)	± 10 bar	± 3 bar	± 10 bar	± 4 bar

710 Table A-6: Fitted coefficients of Equation 5 for the determination of density (at 32 °C) of CO_2-
711 N_2 gas mixtures. The uncertainty (1σ) of the calibration polynomial equation of each range is listed in
712 the last row.

PX domains / c_{ij}	50-100 mol% CO_2		10-50 mol% CO_2	
	5-600 bar	5-160 bar	5-600 bar	5-160 bar
c00	0.322557	0.014508	0.052969	0.032500
c10	–1.373203	–0.086464	–0.591457	–0.361537
c01	1.982120	2.409656	2.418676	2.738940
c20	1.901505	0.152268	2.021816	1.267886
c11	–5.113733	–6.734110	–8.676565	–11.352661
c02	0.073184	–0.116314	–0.998621	–1.873395
c30	–0.848128	–0.074937	–2.112004	–1.359611
c21	5.307588	7.477710	11.215350	17.034457
c12	0.589915	0.807514	6.539504	16.500441
c03	–0.209968	–0.136942	–0.392779	–5.356779
c31	–1.909427	–2.902051	–2.564151	–5.818552
c22	–0.462021	–0.460642	–8.685633	–26.584920
c13	0.135753	0.040956	1.017467	13.567035
c04	0.006276	0.011606	–0.138500	–1.565370
Adjusted R^2	0.9996	0.9996	0.9996	0.9950
Uncertainty (1σ)	± 0.006	± 0.006	± 0.005	± 0.005

713

Table A-7: Fitted coefficients of Equation 5 for the determination of pressure (at 22 °C) of CO_2-N_2 gas mixtures. The uncertainty (1σ) of the calibration polynomial equation of each range is listed in the last row.

PX domains / c_{ij}	50-100 mol% CO_2		10-50 mol% CO_2	
	5-600 bar	5-160 bar	5-600 bar	5-160 bar
c00	–137.742	88.967	1.955	8.931
c10	683.702	–377.311	147.811	–50.301
c01	1930.147	1118.943	1682.405	1814.667
c20	–1089.503	522.272	–844.985	29.398
c11	–6950.342	–2680.493	–9024.047	–7550.765
c02	865.542	121.155	1402.170	–406.409
c30	547.846	–233.627	1091.816	70.929
c21	10147.692	2796.365	26032.684	17082.171
c12	–3537.190	–757.074	–11773.206	–6973.173
c03	600.002	204.249	2319.004	5905.099
c31	–4980.751	–1072.487	–26651.658	–15617.520
c22	2557.165	552.456	17438.386	15041.744
c13	–624.148	–267.490	–4651.095	–11712.853
c04	28.644	38.666	205.721	44.608
Adjusted R^2	0.9990	0.9986	0.9994	0.9955
Uncertainty (1σ)	±7 bar	±3 bar	±8 bar	±3 bar

Table A-8: Fitted coefficients of Equation 5 for the determination of density (at 22 °C) of CO_2-N_2 gas mixtures. The uncertainty (1σ) of the calibration polynomial equation of each range is listed in the last row.

PX domains / c_{ij}	50-100 mol% CO_2		10-50 mol% CO_2	
	5-600 bar	5-160 bar	5-600 bar	5-160 bar
c00	0.376216	0.010280	0.035844	0.011260
c10	–1.740868	–0.064068	–0.397086	–0.070292
c01	1.490436	2.626929	1.877266	2.107761
c20	2.561821	0.127033	1.398697	0.065704
c11	–2.248784	–8.142853	–4.921546	–7.480476
c02	–0.234697	0.523089	–0.713235	–0.621856
c30	–1.200926	–0.074232	–1.505246	0.061639
c21	0.665529	9.839291	2.879115	15.938249
c12	1.201509	–0.367180	5.144878	–6.107679
c03	–0.169712	–0.348974	–0.405858	6.501687
c31	0.405396	–3.991261	3.153925	–14.697989
c22	–0.884667	–0.209187	–6.276756	16.066299
c13	0.171749	0.469233	0.431299	–13.570084
c04	–0.007822	–0.035452	0.005927	0.072953
Adjusted R^2	0.9999	0.9999	0.9997	0.9953
Uncertainty (1σ	±0.004	±0.003	±0.004	±0.004

Appendix B: Detailed calculation procedure of *PVX* properties and estimation of global uncertainty

B.1 Estimation of global uncertainty of the measured composition

The composition of CO_2 (X_{CO_2}) within CO_2-CH_4 mixtures can be calculated by Equation 6 from the CO_2 and CH_4 peak area (A_{CO_2} and A_{CH_4}) and the corresponding RRSCS (σ_{CO_2} and σ_{CO_2}). Thus, the standard uncertainty of the measured X_{CO_2} ($i_{X_{CO_2}}$) combining the uncertainty of every variable in Equation B-1 (i.e., $i_{A_{CH_4}}$, $i_{A_{CO_2}}$, $i_{\sigma_{CH_4}}$, and $i_{\sigma_{CO_2}}$) can be calculated by Equation B-2. The calculation of the composition of other binary mixtures or ternary mixtures and the associated uncertainties can be done similarly.

$$X_{CO_2} = \frac{\frac{A_{CO_2}}{\sigma_{CO_2}}}{\frac{A_{CO_2}}{\sigma_{CO_2}} + \frac{A_{CH_4}}{\sigma_{CH_4}}} \quad \text{B-1}$$

$$i_{X_{CO_2}} = \sqrt{\left(\frac{\partial X_{CO_2}}{\partial A_{CH_4}}\right)^2 \cdot (i_{A_{CH_4}})^2 + \left(\frac{\partial X_{CO_2}}{\partial A_{CO_2}}\right)^2 \cdot (i_{A_{CO_2}})^2 + \left(\frac{\partial X_{CO_2}}{\partial \sigma_{CH_4}}\right)^2 \cdot (i_{\sigma_{CH_4}})^2 + \left(\frac{\partial X_{CO_2}}{\partial \sigma_{CO_2}}\right)^2 \cdot (i_{\sigma_{CO_2}})^2} \quad \text{B-2}$$

B.2 Pure systems of CO_2 and CH_4

The calculation procedure of pure systems (CO_2 and CH_4) is relatively straightforward because it involves only one regression calibration equation for the entire density or pressure range at a fixed temperature. Figure B-1a and b present the user interface of the calculation module of the pure CO_2 and CH_4, respectively. The temperature used in the experiments must be selected (22 or 32 °C) before entering the other spectroscopic data in the INPUT fields of the calculation module. Namely, the required spectral parameters of the pure CH_4 calculation module are "ν_1_sample", "ν_1_std" and "uncertainty", which are respectively the *relative* variation of the CH_4 ν_1 band ($\nu^*_{CH_4}$) of the sample and of the standard at near-zero pressure (density) ($\nu^0_{CH_4}$), and the associated uncertainty (e.g., ~ ±0.02 cm^{-1} for the measurements performed in this study).

Regarding the module of pure CO_2, the calculation is based on the CO_2 Fermi diad splitting and its uncertainty (Figure B-1a). It is to note that only the absolute value of the CO_2

Fermi diad splitting (Δ_{CO_2}) is needed for the pressure and density determination when the analysis is performed using the LabRAM HR ("Dassin") spectrometer at GeoRessouces laboratory. When using other spectrometers, the calculation is based on the relative variation of the CO_2 Fermi diad splitting ($\Delta^*_{CO_2}$). A standard sample containing less than ~ 5 bar of CO_2 is therefore needed to measure the value of the CO_2 Fermi diad splitting at near-zero pressure ($\Delta^0_{CO_2}$).

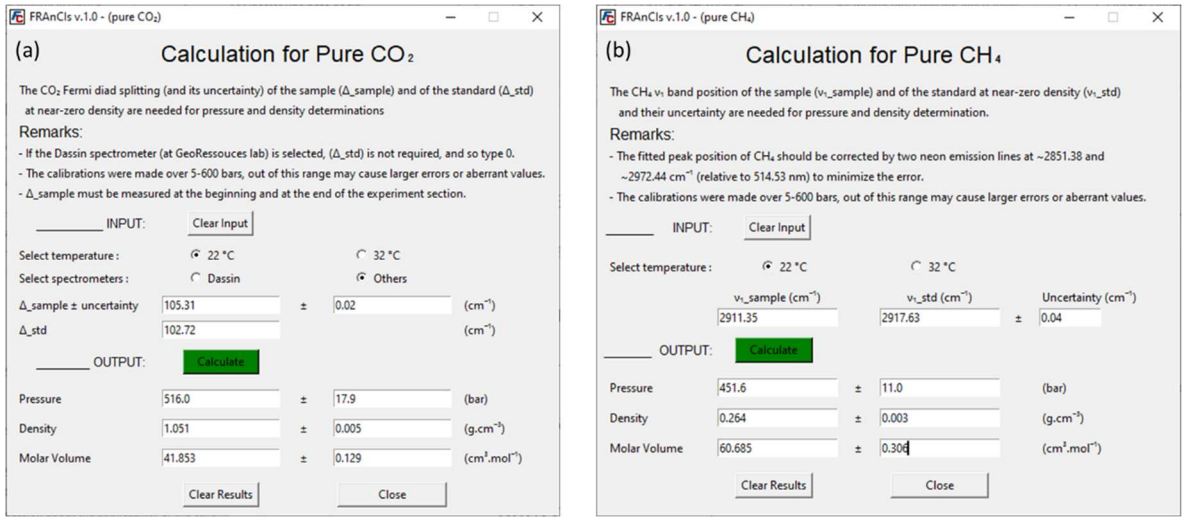

Figure B-1: User interface of the calculation module of (a) pure CO_2 and (b) pure CH_4 with an example of the calculation of *PVX* properties from spectroscopic data recorded at 22 °C.

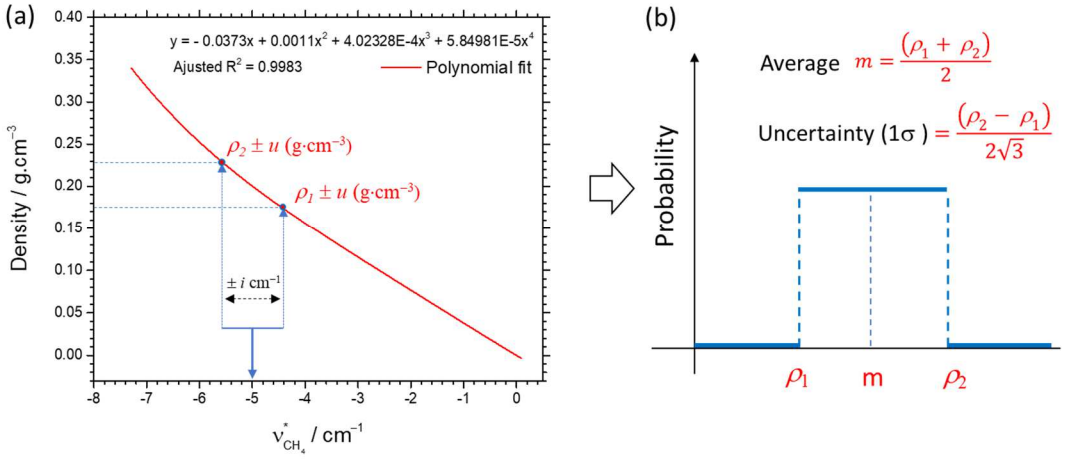

Figure B-2: Calculation procedure of pure CH_4 module (a) Error propagation arising from the uncertainty of a given band position of CH_4 (± **i**) and of the regression calibration equation (± **u**). The red-solid line is the regression equation fitted from experimental data. (b) Probability function according to the rectangular distribution. Indeed, the probability of the density calculated from a given

$\nu^*_{CH_4} \pm$ i (cm^{-1}) falls between ρ_1 and ρ_2 ($g \cdot cm^{-3}$) is always the same. Otherwise, the probability is equal to zero.

Figure B-2a presents the schema of the error propagation upon the calculation procedure of the density of pure CH_4 system from $\nu^*_{CH_4}$. Indeed, for a given $\nu^*_{CH_4}$ measured with an uncertainty of ± i (1σ), the calculated density is expected to fall between ρ_1 and ρ_2, where ρ_1 and ρ_2 are the densities derived respectively from ($\nu^*_{CH_4} + i$) and ($\nu^*_{CH_4} - i$) using the regression equation. Herein, the rectangular distribution is used because of its simplicity, and it gives the largest standard deviation (compared to others, e.g., the normal or triangular distributions). The distribution function of the expected densities is described in Figure B-2b. Thereby, the average density (m) and the uncertainty (i^*) arising from the first error source i (i.e., the uncertainty of the measured spectral parameter $\nu^*_{CH_4}$) can be calculated using Equation B-3 and B-4, respectively.

$$m = \frac{\rho_1 + \rho_2}{2} \qquad \text{B-3}$$

$$i^* = \frac{\rho_2 - \rho_1}{2\sqrt{3}} \qquad \text{B-4}$$

Furthermore, both densities ρ_1 and ρ_2 that were derived from the regression polynomial equation contain already an uncertainty ± u (1σ), e.g., the second error source. Thus, there is additional uncertainty (u^*) of the average density (m). The uncertainty u^* can be calculated using Equation B-5. Finally, the final uncertainty is the sum of two error sources, e.g., $i^* + u^*$ (Fall et al., 2011; Wang et al., 2011). The calculation procedure for pure CO_2 is identical to that of CH_4.

$$u^* = \sqrt{\left(\frac{\partial m}{\partial \rho_1}\right)^2 \cdot (u)^2 + \left(\frac{\partial m}{\partial \rho_2}\right)^2 \cdot (u)^2} \qquad \text{B-5}$$

B.3 Binary systems: CO_2-N_2, CH_4-N_2, and CO_2-CH_4 mixtures

The calculation procedure and the uncertainty estimation for the binary mixtures are slightly more complex because there are two variables in each regression calibration equation (e.g., the measured composition, and the CO_2 Fermi diad splitting or the variation of the CH_4 band position). To minimize the uncertainty associated with the second error source (u), different regression equations were individually fitted from experimental data over a specific

785 composition-pressure range. Overall, the regression equations of binary mixtures were fitted
786 for four smaller pressure-composition ranges, i.e., > 50 mol% or < 50 mol%, and over 5-600
787 bar or over 5-160 bar. The spectral parameters required for the quantitative measurements of
788 each binary system are also different. For instance, due to the modest reproducibility of the
789 spectral parameters of N_2, only the CO_2 Fermi diad splitting (Δ_{CO_2} or $\Delta^*_{CO_2}$) can be used as a
790 reliable parameter for the quantitative measurement of the CO_2-N_2 mixtures. Similarly, only
791 the variation of the CH_4 ν_1 band position ($\nu^*_{CH_4}$) can accurately be used for the CH_4-N_2
792 mixtures (Table 4).

793 Regarding the CO_2-CH_4 mixtures, both Δ_{CO_2} (or $\Delta^*_{CO_2}$) and $\nu^*_{CH_4}$ can be used as reliable
794 spectral parameters for quantitative measurement of pressure and density (Table 4). However,
795 it is to note that the sensibility (as varying of pressure or density) of the Δ_{CO_2} (or $\Delta^*_{CO_2}$) and
796 the $\nu^*_{CH_4}$ decreases with decreasing CO_2 or CH_4 concentration. Therefore, Δ_{CO_2} (or $\Delta^*_{CO_2}$) is
797 used when the concentration of CO_2 > 50 mol%, whereas $\nu^*_{CH_4}$ is used when the
798 concentration of CO_2 < 50 mol% (i.e., > 50 mol% CH_4).

799 Figure B-3 presents the user interface of the module of the CO_2-CH_4 mixtures with an
800 example of a calculation from the spectroscopic data recorded by 514 nm excitation laser and
801 at 32 °C. The spectral parameters required in the CO_2-CH_4 module are the peak areas (A_{CO_2}
802 and A_{CH_4}), $\nu^*_{CH_4}$, Δ_{CO_2} (or $\Delta^*_{CO_2}$) and their uncertainties $i_{\nu^*_{CH_4}}$ and $i_{\Delta_{CO_2}}$. The uncertainty of
803 the fitted peak area is not required because we already assumed, from our statistical analyses,
804 that the uncertainty of the measured composition is about ±0.5 mol% (Equation B-2).

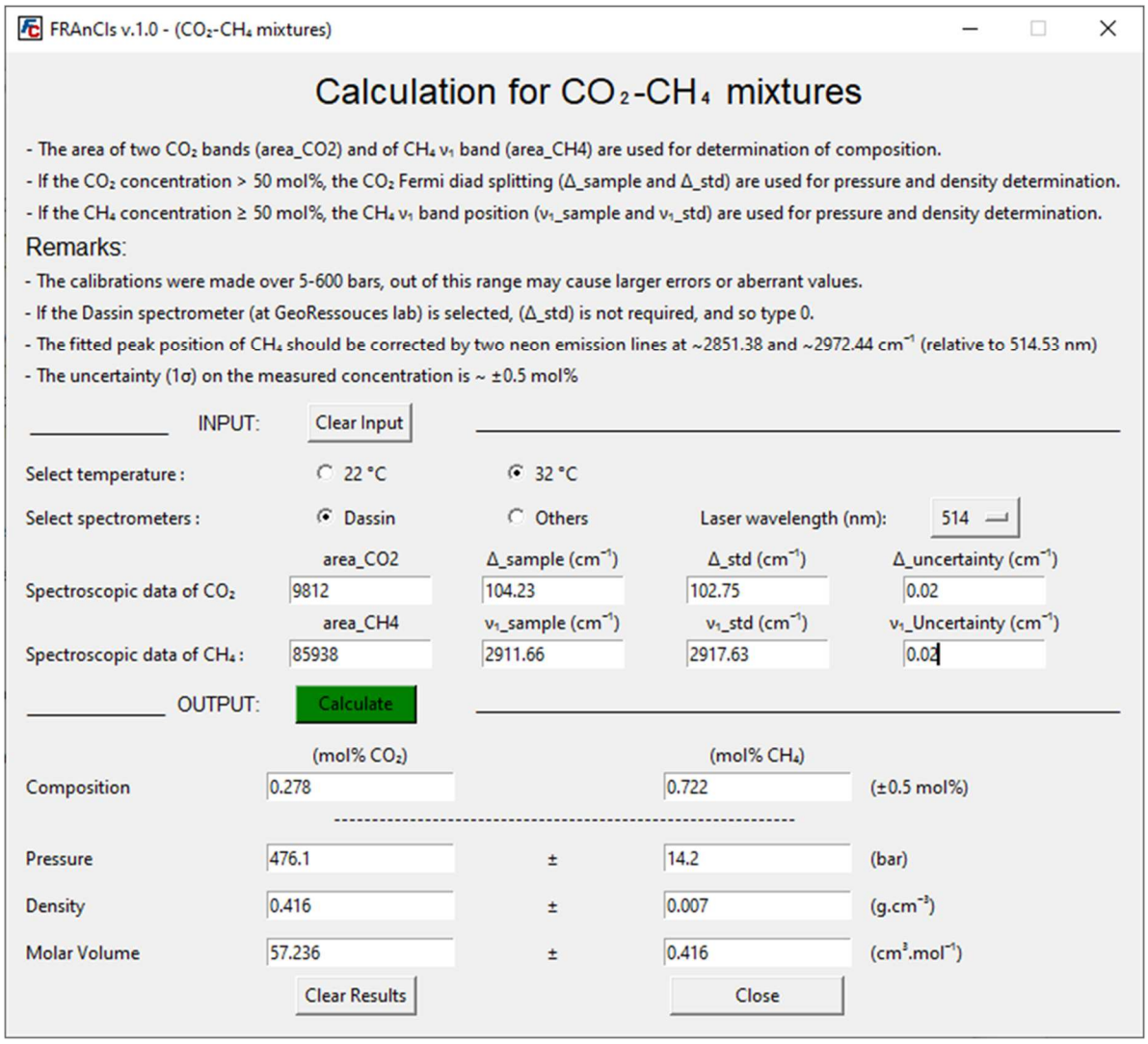

Figure B-3: User interface of the calculation module for CH_4-CO_2 mixtures with an example of measurements and of *PVX* calculation at 32 °C.

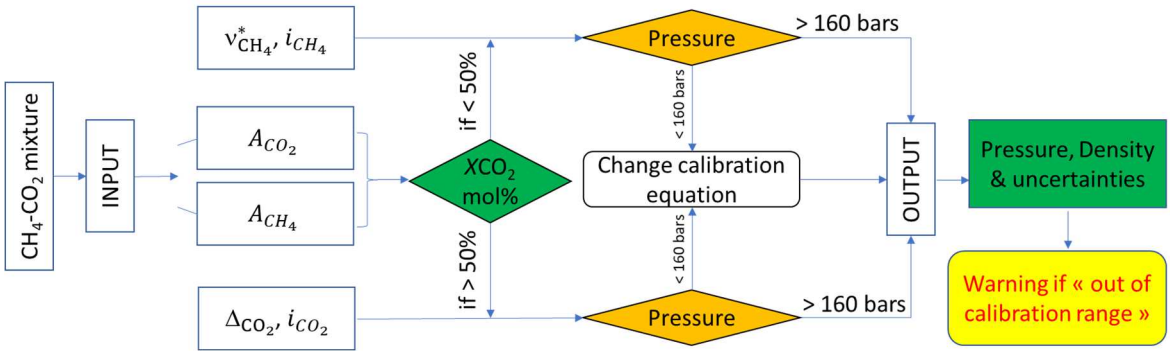

Figure B-4: Schema of the procedure of the *PVX* properties calculation within the module of CO_2-CH_4 mixtures (read text for more detail).

Figure B-4 describes the calculation procedure of the module for CO_2-CH_4 mixtures. Indeed, the composition of CO_2-CH_4 mixtures is firstly calculated from the peak areas and

RRSCS of CO_2 and CH_4 (e.g., 2.29 ± 0.02 and 7.73 ± 0.16, cf. Le et al., 2019, 2020). If the CO_2 concentration is more than 50 mol%, only Δ_{CO_2} and its uncertainty $i_{\Delta_{CO_2}}$ (combined with the obtained concentration) are used for further calculation of pressure, density, and associated uncertainties. In the other cases (< 50 mol% CO_2), $\nu^*_{CH_4}$ and its uncertainty $i_{\nu^*_{CH_4}}$ are then used.

Then, the appropriate regression calibration equation fitted over the entire studied pressure range (5-600 bar) is automatically selected for the calculation of pressure. If the obtained pressure is > 160 bar, the calculated *PVX* properties and all associated uncertainties are then displayed in the OUTPUT fields. If the calculated pressure is < 160 bar, the *PVX* properties are then re-calculated using another regression equation, which was fitted over a lower pressure range (5-160 bar) to minimize the uncertainty of the measurement further.

The results are then displayed in the OUTPUT fields. If the results are out of the calibration range (cf. Table 4), a pop-up will appear to warn and suggest the user to refer to the related reference for more information.

The calculation procedures of the other binary mixtures (CH_4-N_2 and CO_2-N_2) are similar and can be deduced from the schema presented in Figure B-4. The only difference is that only Δ_{CO_2} (or $\Delta^*_{CO_2}$) is required for the calculation within the CO_2-N_2 mixtures, and only $\nu^*_{CH_4}$ is required for the calculation within the CH_4-N_2 mixtures.

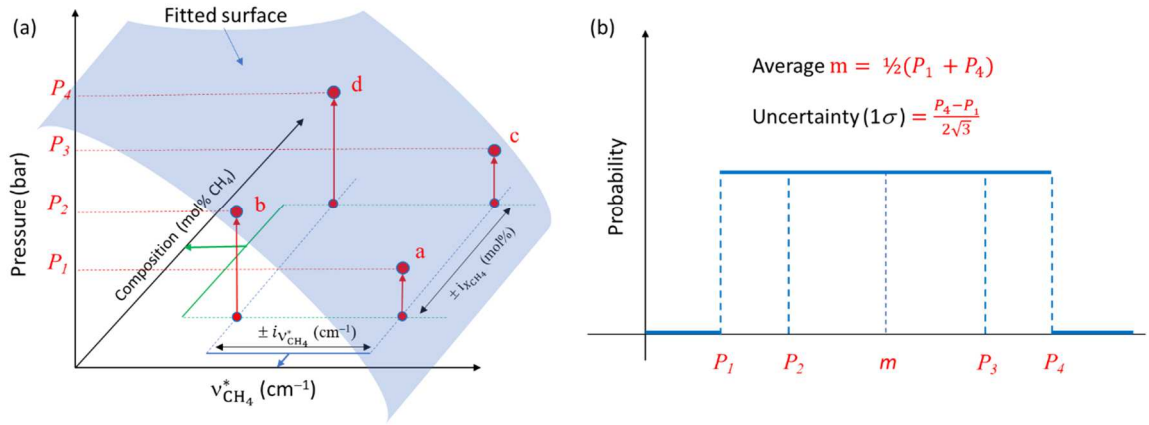

Figure B-5: (a) Illustration of the error propagation arising from the uncertainty $\pm\, i_{\nu^*_{CH_4}}$ (of the $\nu^*_{CH_4}$) and the uncertainty $\pm\, i_{C_{CH_4}}$ (of the measured composition X_{CH_4}). (b) Probability of the expected pressure (or density) according to the rectangular distribution. The pressure (or density) is calculated from a given ($\nu^*_{CH_4} \pm i_{\nu^*_{CH_4}}$) and ($X_{CH_4} \pm i_{C_{CH_4}}$), and is expected to fall between P_1 (min) and P_4 (max) with the same probability. Otherwise, the probability is equal to zero.

Figure B-5a illustrates the error propagation upon the pressure calculation of the CH_4-N_2 binary mixtures. Indeed, the pressure calculated from a given composition ($X_{CH_4} \pm i_{C_{CH_4}}$) and a given peak position ($\nu^*_{CH_4} \pm i_{\nu^*_{CH_4}}$) using the regression polynomial calibration equation is expected to fall within a "*rectangular*" limited by four extremes (a, b, c and d) on the fitting surface Figure B-5a. This means that the calculated pressure ranges from P_1 to P_4, where P_1 and P_4 are respectively the maximal and minimal possible values. Similarly, the rectangular distribution is also used herein to calculate the average value of the final pressure and to estimate the global uncertainty (Figure B-5b). According to the rectangular distribution function, the average pressure (or density) and the associated uncertainty can be calculated using Equation B-6 and B-8, respectively. The calculation of density and its uncertainty within the binary mixtures are similar to that of pressure and so not described herein.

$$P = \frac{P_1 + P_4}{2} \quad \text{B-6}$$

$$i^* = \frac{P_4 - P_1}{2\sqrt{3}} \quad \text{B-7}$$

$$u^* = \sqrt{\left(\frac{\partial P}{\partial P_1}\right)^2 \cdot (u)^2 + \left(\frac{\partial P}{\partial P_4}\right)^2 \cdot (u)^2} \quad \text{B-8}$$

It is to note that all pressure or density of the binary mixtures derived from a given composition and $\nu^*_{CH_4}$ using the regression calibration data also contains a certain uncertainty "u" (e.g., the second error source as described above). Therefore, the average pressure (or density) calculated from Equation B-6 must have an additional uncertainty (u^*) calculated using Equation B-8. The global uncertainty in the final pressure or density is thereby the sum of two error sources, i.e., ($i^* + u^*$).

B.4 Ternary system: CO_2-CH_4-N_2

Figure B-6 presents the user interface of the calculation module of CO_2-CH_4-N_2 ternary mixtures with an example of calculation at 32 °C using an excitation laser of 514 nm. All required spectral parameters are the peak areas of CO_2, CH_4 and N_2 bands and the CO_2 Fermi diad splitting (and its uncertainty). Since the variation of the CH_4 ν_1 band position ($\nu^*_{CH_4}$) cannot be used for the determination of the pressure and density of the ternary mixtures, only the CO_2 Fermi diad splitting (Δ_{CO_2} for the Dassin spectrometer (GeoRessources Lab, France)

or $\Delta^*_{CO_2}$ for other spectrometers) is thus used for the entire composition range, even when the concentration of CO_2 is less than 50 mol%.

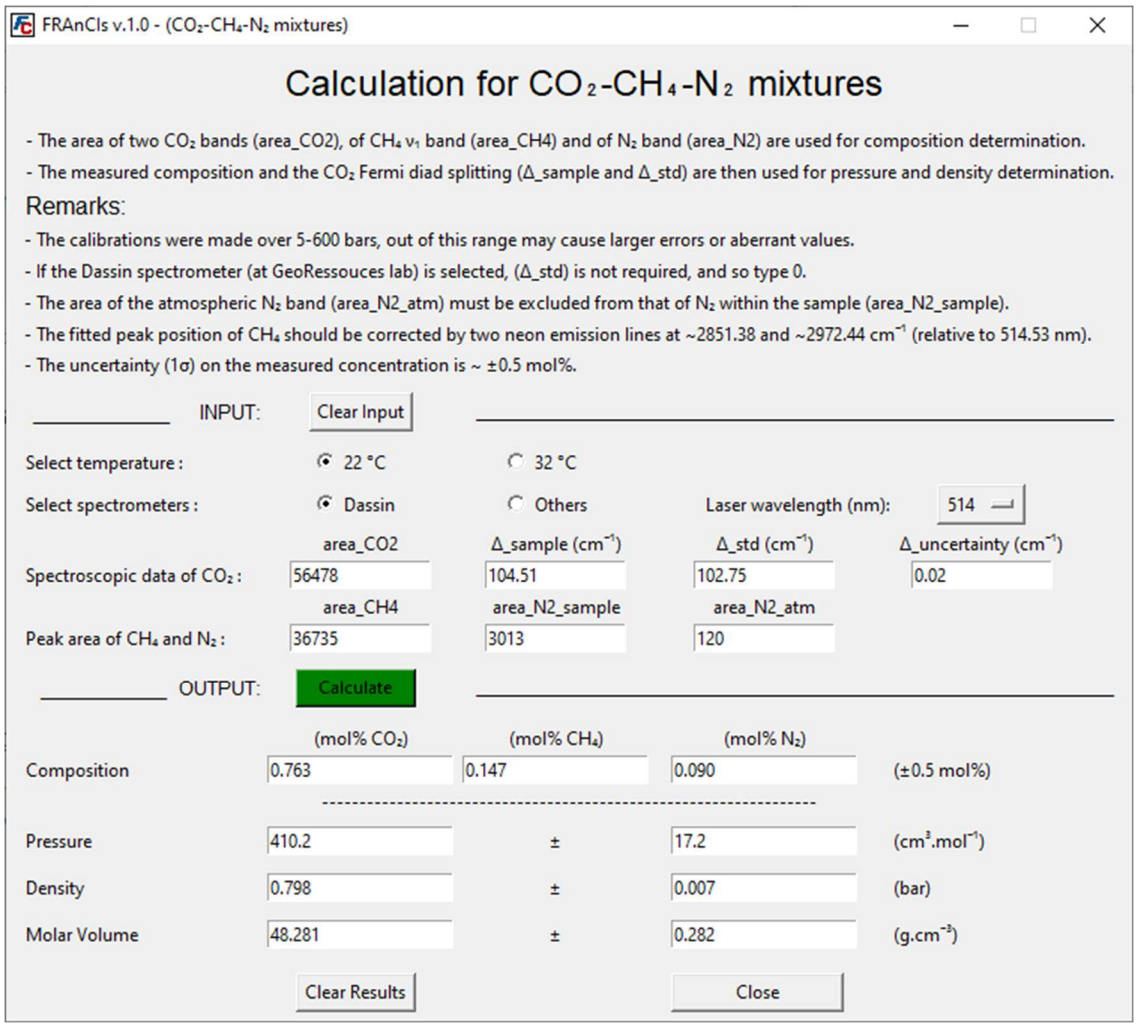

Figure B-1: User interface of the calculation module for ternary CH_4-CO_2-N_2 mixtures with an example of measurements and of *PVX* calculation at 32 °C.

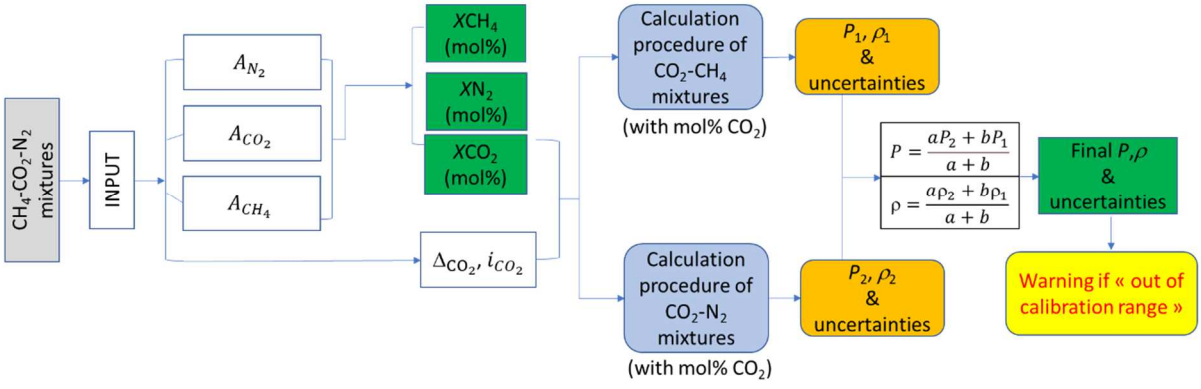

Figure B-7: Calculation procedure for the *PVX* properties determination within the module of CO_2-CH_4-N_2 ternary mixtures.

Figure B-7 presents the scheme of the calculation procedure within the module developed for the CO_2-CH_4-N_2 ternary mixtures. The composition of the ternary mixtures (XCO_2, XCH_4 and XN_2) is firstly calculated from the peak area of CO_2, CH_4, and N_2 (A_{CO_2}, A_{CH_4} and A_{N_2}) and their RRSCSs (e.g., 2.29 ± 0.02, 7.73 ± 0.15, and 1, respectively). The pressure and the density of the ternary mixtures (P and ρ) are then calculated from the CO_2 composition (XCO_2) and the CO_2 Fermi diad splitting (Δ_{CO_2} or $\Delta^*_{CO_2}$ depending on the used Raman spectrometer).

Pressure P (or density ρ) of the ternary mixtures was demonstrated to be always between pressure P_1 and P_2 (or density ρ_1 and ρ_2) of the CO_2-CH_4 and CO_2-N_2 binary mixtures, respectively, with P, P_1 and P_2 (or ρ, ρ_1 and ρ_2) all measured from a given XCO_2 and Δ_{CO_2} (or $\Delta^*_{CO_2}$). Therefore, the calculation procedure of the pressure P (or density ρ) of the ternary mixtures involves two individual calculations of P_1 (or ρ_1) and P_2 (or ρ_2) (Figure B-7).

For instance, considering here the determination of pressure P (or density ρ) of the ternary mixture of 80-a-b mol% (XCO_2-XCH_4-XN_2) with $a + b = 20$ mol%, the program will process two calculation procedures for the determination of the pressure P_1 and P_2 (or density ρ_1 and ρ_2) of the binary mixtures of 80 mol% CO_2 (, i.e., CO_2-CH_4 (80-20) and CO_2-N_2 (80-20), respectively) from the measured value of Δ_{CO_2} (or $\Delta^*_{CO_2}$) within the analyzed ternary mixture. Once the pressure P_1, P_2 are calculated, the pressure P of the ternary mixtures is then deduced from the molar proportion of CH_4 and N_2 within the ternary mixture (e.g., a and b mol%, respectively) using Equation B-9 (see Le et al. (2020) for more detail). Similarly, the density ρ of the ternary mixtures can be calculated from ρ_1 and ρ_2 and the molar proportions a and b using Equation B-10.

The global uncertainty of P, P_1 and P_2 (or of ρ, ρ_1 and ρ_2) can be calculated by following the calculation procedure described for the binary mixtures in the previous subsection (cf. Equations B-4, B-5, B-7 and B-8).

$$P = \frac{aP_2 + bP_1}{a + b} \qquad \text{B-9}$$

$$\rho = \frac{a\rho_2 + b\rho_1}{a + b} \qquad \text{B-10}$$